Wesleyan University The Honors College

# Absorption of Carbocyanine Dyes Bound to Quadruplex DNA

by

Andrew Harry Marvin-Smith
Class of 2008

A thesis submitted to the
faculty of Wesleyan University
in partial fulfillment of the requirements for the
Degree of Bachelor of Arts
with Departmental Honors in Chemistry

Middletown, Connecticut April, 2008

**TABLE OF CONTENTS**

Acknowledgements……...…..…3

Abstract……..……..…4

Introduction……..……5

Materials and Methods...……15

Results and Discussion……...……20

References……..……52

Acknowledgements

First and foremost I would like to thank my advisor, Professor Bolton, for the opportunity to participate in his research team for the past two years. I would like to thank Nathan for his willingness to help me whenever I needed it; this thesis would have certainly been impossible without him. I would like to thank my parents for their limitless support and encouragement throughout my college years; thank you for giving me the confidence to set goals and go after them. I would like to thank my roommates and friends for their tolerance, encouragement, and admonishment. Last but not least, I would like to thank Sally Bronson.

Abstract

Telomeres and telomerase have become the focus of a growing branch of research because of their involvement in the ability of tumor cells to replicate indefinitely. One area of this research is the study of the structure and function of G-quadruplexes. It has been previously shown that the telomeric DNA sequence "chosen" by evolution possesses the ability to fold into quartets under intracellular conditions, which could be the reason that evolution selected for that sequence. Nonetheless, the direct evidence of quadruplexes *in vivo* is scarce. In order to enhance the understanding of the presence and role of quadruplexes in cellular function, I investigate the selectivity of two carbocyanine dyes in their binding to several different quadruplex structures through the absorption of the dye molecule. Finding quadruplex ligands that bind selectively among the many different quadruplexes is paramount to this area of research. Binding modes appear to differ between the dyes and among the DNA quadruplexes. Significant changes in the wavelength and intensity of maximum absorbance were observed.

Introduction

The termini of a chromosome present two unique problems. Cells need to overcome the loss of DNA caused by the end-replication problem (Figure 1) (1, 2). The shortening of a chromosome due to the end-replication problem is exacerbated in tumor cells because of their unlimited potential for cell division (3). In addition, the ends of a linear chromosome appear as a double strand break to DNA repair systems (4). Both of these problems are solved by telomeres, the specialized structures that exist at the termini of linear DNA, and the telomere-associated proteins (5, 6).

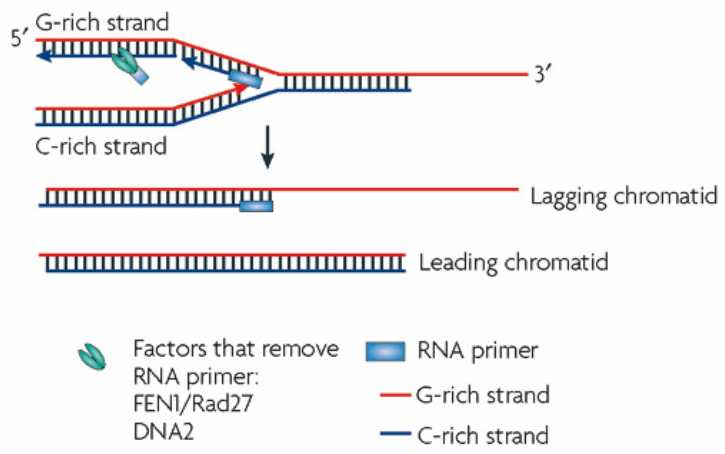


**Figure 1.** The end replication problem.

The DNA portion of the normal human telomere consists of several kilobases of repeats of the same sequence (7). The repeated sequence varies among species but is always dG-rich on the 3' strand (8). Part of the telomere is a double helix, and there is a short 3' overhang of dG-rich single-stranded DNA (9).

Before a chromosome is copied, a replication initiator protein binds to, and separates, the double-stranded DNA at one of approximately 40,000 origins (10). Helicase enzymes continue the separation of the double helix by breaking the

hydrogen bonds that hold it together, creating a replication bubble, while topoisomerase relieves the built-up tension of the rotating DNA (Figure 2) (11, 12). DNA polymerase α (pol α) binds to the ssDNA at the origin and synthesizes approximately 10 nucleotides of RNA followed by 20-30 nucleotides of DNA, both in the 5'-3' direction (10). The proliferated cell nuclear antigen (PCNA) then dissociates pol α and facilitates the binding of polymerase δ (pol δ) and flap structure-specific endonuclease 1 (FEN1) (10). Pol δ synthesizes DNA 5'-3' until it reaches the RNA primer synthesized at the adjacent initiation event. At this point FEN1 removes an RNA one nucleotide at a time as pol δ replaces it with DNA (10). The end-replication problem occurs at the 3' end of the existing DNA sequence (1, 2). The RNA primer synthesized by pol α at the 3' end is not replaced with DNA by pol δ because there is no adjacent initiation event. The 5' end of the new strand will be at least one primer short, but the loss is usually closer to 50 nucleotides (13). Cells solve the end-replication problem partially because the telomeres do not contain any coding information (14).

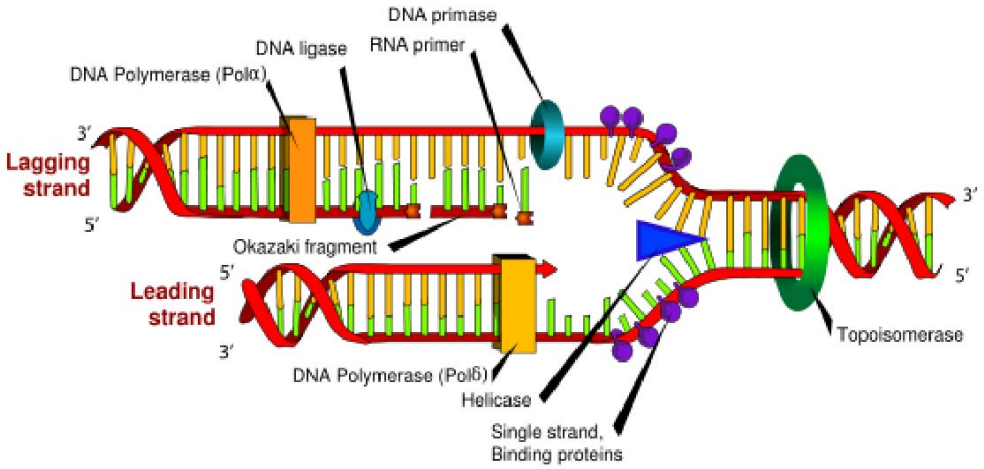


**Figure 2.** DNA replication.

The progressive loss of DNA is a fundamental problem of linear chromosomes; each cell cycle shortens the chromosome (15). When the telomere shortens to a critical length the cell enters a state of permanent growth arrest called replicative senescence (15). Normal human cells divide at most 32 times during a lifetime. If senescence is bypassed, such as by inactivation of tumor suppressor genes, the telomeres are shortened further (15). This can lead to chromosome instability and apoptosis (15). Telomere shortening in adult stem cells is partially responsible for deficient tissue regeneration (16). This time dependent cell malfunction may be a contributor to cell aging (17). However, if a cell can lengthen its telomere, telomere erosion and replicative senescence can be avoided. For example, human skin and intestinal cells lengthen their telomeres and are thus able to divide throughout an individual's entire lifespan.

Telomerase is a reverse transcriptase enzyme which lengthens the telomere (14). The enzyme consists of a protein, human telomerase reverse transcriptase (hTERT); an RNA sequence, human telomerase RNA (hTR or hTERC); and dyskerin (18). The RNA sequence for replication is 3'-CAAUCCCAAUC-5', which is nearly two repeats of the complement to the 3' tail (19). The first five nucleotides bind to the end of the 3' overhang, and the protein component reverse transcribes an additional repeat sequence onto the telomere using the RNA as a template (14). The ability of telomerase to extend a piece of ssDNA is based upon its captive RNA (20). Whereas DNA polymerase uses an existing strand of DNA as a template, telomerase supplies its own template, hTERC.

While telomerase is active at low levels in most cells, it is active in germ cells and approximately 85% of tumor cells (14). Telomerase activity is a trait that helps endow most of them with their ability to replicate indefinitely (14). Inhibiting telomerase activity in tumor cells can inhibit telomere lengthening and produces a normal cellular lifespan (14). Some of the remaining 15% of tumor cells extend their telomeres without the aid of telomerase through the alternative lengthening of telomeres (ALT) mechanism (21, 22). It has been proposed that telomere replication through the ALT pathway is dependent upon homologous recombination (23). ALT activity has been observed in mouse and human tumor cell-lines and human somatic cells immortalized *in vitro* (21, 22, 24, 25), which suggests that the ALT mechanism is reserved for cells experiencing telomere recombination dysfunction (15).

In addition to solving the end-replication problem, telomeric DNA and telomere associated proteins protect the ends of the chromosome (15). Without proper protection mechanisms, the end of a chromosome would be recognized as a double-strand break (15). This can lead to checkpoint activation, non-homologous end joining of two chromosomes, or homologous recombination (13). The mere existence of telomeric DNA does not protect the chromosome; there are many proteins involved (Figure 3).

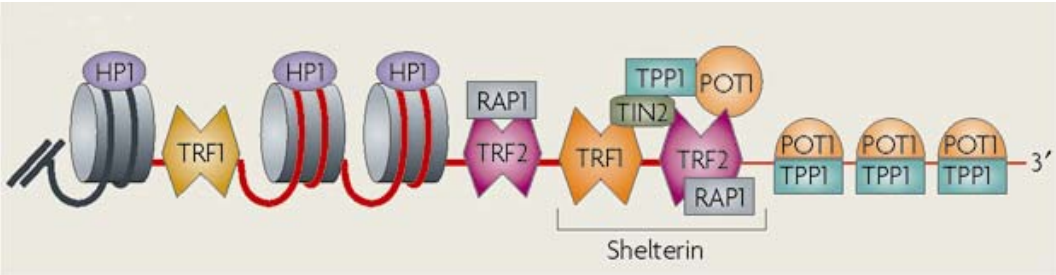


**Figure 3.** Telomere associated proteins. The thick red line represents duplex DNA telomere repeats and the thin red line represents the ssDNA G-tail.

The majority of double stranded telomeric DNA is packaged similarly to the rest of the chromosome in nucleosomes (13). Heterochromatin protein-1 (HP1) is involved in these telomere nucleosomes (13). Shelterin is a complex comprised of six telomere-associated proteins (13). TTAGGG-repeat factor-1 (TRF1) and TTAGGG-repeat factor-2 (TRF2) bind to double-stranded telomeric DNA (13). Protection of telomeres protein-1 (POT1) binds to the 3' overhang (13). TRF1-interacting factor-2 (TIN2), POT1 binding partner (TPP1), and repressor activator protein-1 (RAP1) shape the telomere and shelterin complex by binding among the other three proteins (13). POT1 and TPP1 also form heterodimers on the 3' overhang (13). It has been theorized that one function of the shelterin complex is "opening" and "closing" the 3' overhang (Figure 4) (14). In a closed state the 3' overhang is bound into a telomere loop (t-loop) by the shelterin complex and is inaccessible to telomerase and other repair mechanisms. In an open state, all the shelterin complex proteins are present, but the 3' overhang is unbound and accessible.

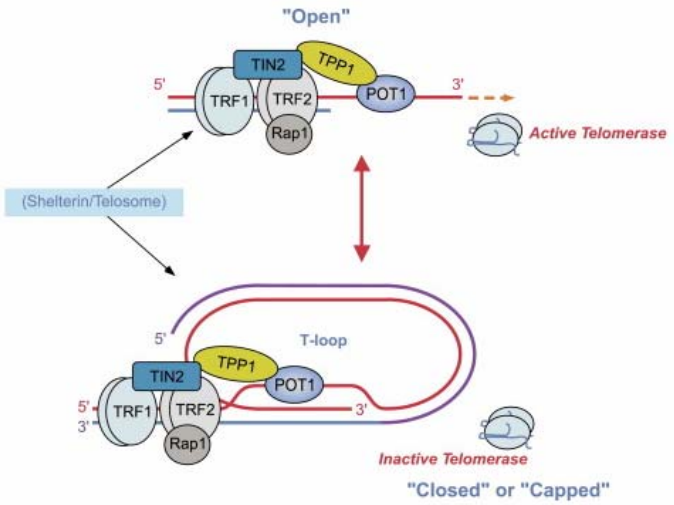


**Figure 4.** Open/closed shelterin complex.

Telomere associated proteins are not the only protection that a telomere provides to a chromosome. Telomeres possess a special trait that could explain why the repeat sequence is TTAGGG and not any one of the multitude of other possibilities. The dG-rich single strand overhang of telomere DNA can form single-, double-, and quadruple-stranded quartets (also known as G4 and G-quadruplex) (26). The quadruplex structures are formed by eight Hoogsteen hydrogen bonds between the dG residues (Figure 5) (14).

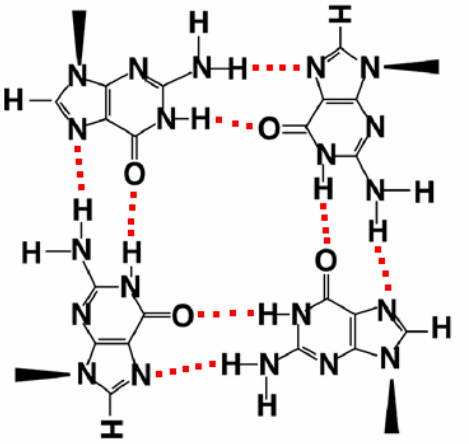

**Figure 5.** dG quartet; Hoogsteen hydrogen bonds in red.

Some quadruplex structures appear to require a cation such as potassium or sodium for stabilization (14). Tetramer quadruplexes consist of four parallel strands in *anti* conformation, but monomer and dimer quadruplexes can be formed by both parallel and antiparallel sequences and in both *syn* and *anti* conformations (Figure 6) (27). In addition to a presence in the telomere, there is evidence that G-quadruplexes form in other parts of the chromosome (28). With over 40% of human promoter genes exhibiting potential quadruplex motifs, it is possible that quadruplex formation is involved in gene regulation at the transcription level (28).

Ligands that bind to quartets have been observed at the telomere *in vivo*, but the role of quadruplexes in the telomere is still unknown (14). A possible function of the dG quartet is the regulation of telomerase activity (14). For telomerase to act

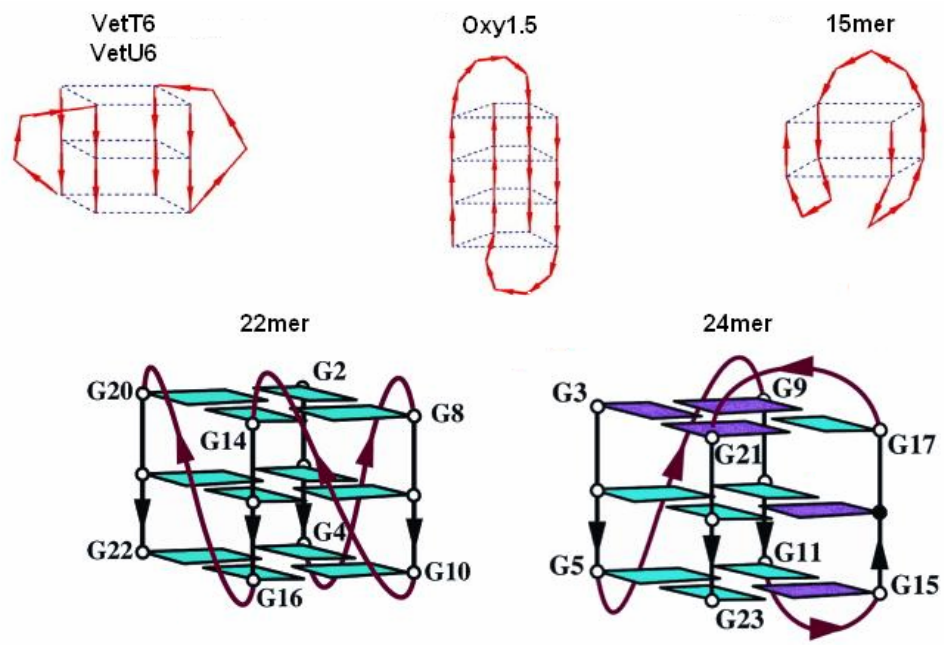


**Figure 6.** G-quadruplex structures. Not to scale. Structures of Vet4 and VetT4 unknown.

upon a telomere, the G-tail must be available for binding to hTERC. If the G-tail forms a quadruplex, then hTERC can not bind (Figure 7). This is supported by the fact that ligands that bind to, and consequently stabilize, quartets inhibit telomerase (29). It has been shown that telomerase extends the telomere 3' overhang and can pause when there are four unassociated repeats. At that point, the four repeats can form a quadruplex and telomerase is inhibited. This is possible because telomerase extends the telomere in an iterative fashion; it binds, synthesizes a repeat, and "jumps" to its next binding site, which it previously synthesized.

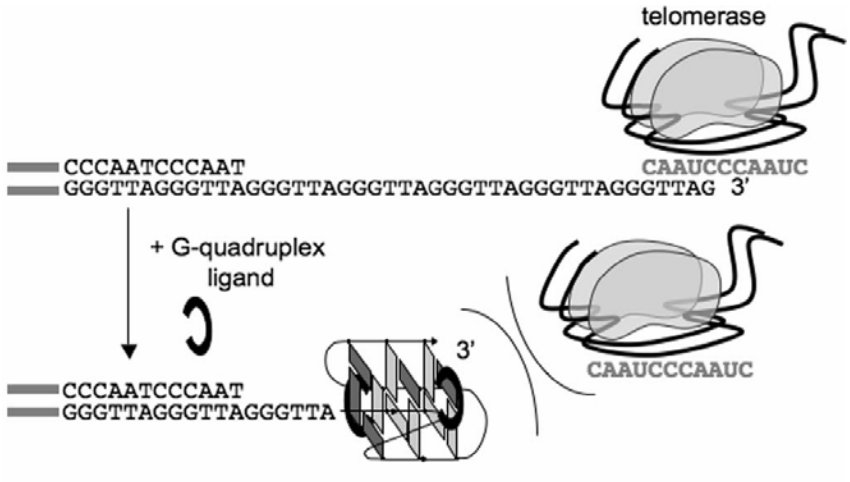


**Figure 7.** Proposed method of telomerase inhibition by ligand stabilized G-quadruplex

It is also possible that G-quadruplexes are involved in telomere maintenance. It has been shown that quartet-binding ligands are selectively toxic to tumor cells (30). The toxicity appears to be independent of telomere shortening because apoptosis occurs before telomere length becomes critical (30, 31). It is more likely that the ligands stabilize G-quadruplexes to the point that telomere maintenance is fatally interrupted (14).

Also, it has been proposed that quadruplex DNA plays an integral role in Werner's syndrome and Bloom's syndrome (32). These disorders are caused by mutations in genes that code for members of the RecQ family of helicases, which can unravel G-quadruplex structures (32). It is possible that the effects of Bloom's syndrome are caused by the failure to properly unwind G4 DNA by the absent RecQ helicase (33) .

Despite the abundance of research on telomeres and G-quadruplex DNA, little is known about which quadruplex structures are present *in vivo* (14). Also, there is

the question of where and when the different structures are present. The goal of my research is to determine if a known quadruplex binding ligand is selective to different quadruplex structures.

3,3'-diethyloxadicarbocyanine (DODC) and 3,3'-diethylthiacarbocyanine (DTDC) are carbocyanine dyes (Figure 8).

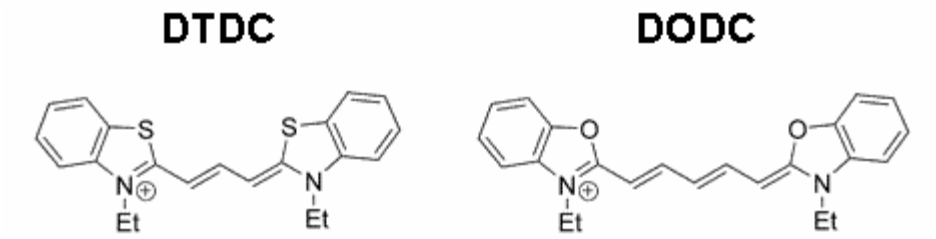


**Figure 8.** Structure of the carbocyanine dyes 3,3'-diethyloxadicarbocyanine (DODC) and 3,3'-diethylthiacarbocyanine (DTDC).

DODC has been shown to interact with G-quadruplexes differently than it does with single strand or duplex DNA. Carbocyanine dyes exist as monomers when alone in methanol solution (34). However, DNA can serve as a template and promote dimerization and aggregation of the dye (34, 35). Offset face-to-face dimers, also known as J-dimers, display absorption bands at shorter wavelengths than the monomer, and straight stacking dimers, also known as H-dimers, display absorption bands at longer wavelengths (Figure 9) (34). Binding of DODC and DTDC to duplex DNA increased absorbance at shorter wavelengths, indicating straight stacking dimerization (34).

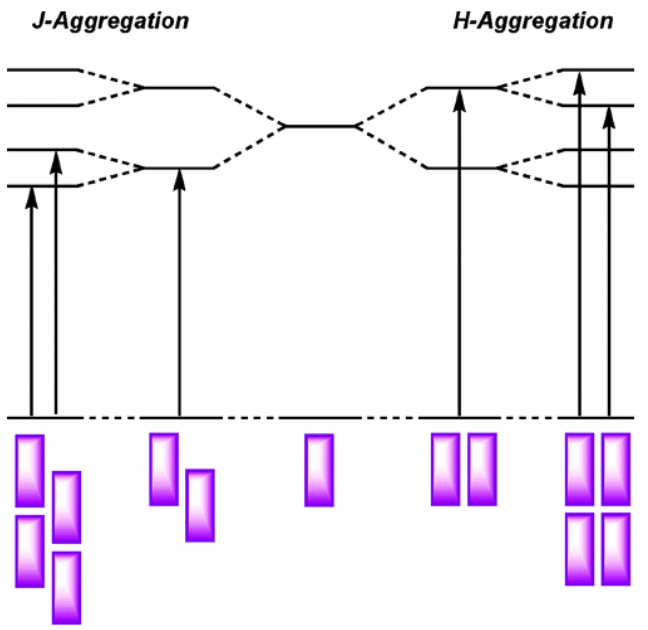


**Figure 9.** Exciton coupling model showing spectral shift based upon aggregate structure.

G-quadruplexes induce spectrophotometric changes in DODC such as a new absorbance peak, a quenching of visible light-excited fluorescence, an induced circular dichroism, and significant energy transfer from DNA (36). Despite the clear evidence that the binding is unique, the mechanism of binding and subsequent cause for the spectrophotometric changes remains largely unknown. My research is aimed at enhancing the understanding of the binding and providing the information necessary to utilize DODC and DTDC as structure specific G-quadruplex probes.

Materials and Methods

| Sequence | Extinction coefficient | Name |
|---|---|---|
| d(TAGGGUTAGGGT) | 121 500 | VetU6 |
| d(TAGGGTTAGGGT) | 122,800 | VetT6 |
| d(TTAGGGTTAGGGTTAGGGTTAGGG) | 244 600 | VetT4 |
| d(GGGTTAGGGTTAGGGTTAGGGTTA) | 246 300 | Vet4 |
| d(AGGGTTAGGGTTAGGGTTAGGG) | 228,500 | 22mer |
| d(GGTTGGTGTGGTTGG) | 143 300 | 15mer |
| d(TTGGGTTAGGGTTAGGGTTAGGGA) | 244,300 | 24mer |
| d(GGGGTTTTGGGG) | 115,200 | Oxy1.5 |

**Table 1**. DNA sample sequences, extinction coefficients, and names.

DODC; DTDC: 3,3'-diethyloxadicarbocyanine (DODC) of 99% purity was purchased from Sigma Aldrich, St. Louis, Missouri. Stock sample was prepared in 99.9% DMSO. The concentration of the stock was determined by absorbance at 582 nm using an extinction coefficient of 270,000.

3,3'-diethylthiadicarbocyanine (DTDC) of 99% purity was purchased from Sigma Aldrich, St. Louis, Missouri. Stock sample was prepared in 99.9% DMSO. The concentration of the stock was determined by absorbance at 560 nm using an extinction coefficient of 125,000.

Buffer: PB3 buffer is 2.5 mM $PO_4$, 5.0 mM $Na^+$, 0.1 mM EDTA, pH 7.0.

PBK buffer is 2.42 mM $PO_4$, 4.83 mM $Na^+$, 97 µM EDTA, 100 mM $K^+$

PB buffer is 20 mM $PO_4$, 140 mM $Na^+$, 0.1 mM EDTA, pH 7.0

VetU6; VetT6: A sample of VetU6, d(TAGGGUTAGGGT), was purchased from Integrated DNA Technologies, Inc., Coralville, Iowa. The HPLC purified sample

was desalted by ethanol precipitation and stored in PB3 buffer. The concentration was determined from the absorbance at 260 nm with the sample at 293 K in distilled water using an extinction coefficient of 121,500. Stock solutions were prepared in PB3 buffer at concentrations of 2 mM, 1 x $10^{-4}$ M, and 4 x $10^{-6}$ M.

A sample of VetT6, d(TAGGGTTAGGGT), was purchased from Integrated DNA Technologies, Inc., Coralville, Iowa. The HPLC purified sample was desalted by ethanol precipitation and stored in PB3 buffer. The concentration was determined from the absorbance at 260 nm with the sample at 293 K in distilled water using the extinction coefficient 122,800. Stock solutions were prepared in PB3 buffer at concentrations of 2 mM, 1 x $10^{-4}$ M, and 4 x $10^{-6}$ M.

From these stock solutions, DNA samples were prepared at concentrations of 2 x $10^{-8}$, 5 x $10^{-8}$, 1 x $10^{-7}$, 2 x $10^{-7}$, 5 x $10^{-7}$, 1 x $10^{-6}$, 2 x $10^{-6}$, 5 x $10^{-6}$, 1 x $10^{-5}$, 2 x $10^{-5}$, 5 x $10^{-5}$, and 1 x $10^{-4}$ M in PBK buffer. To anneal the DNA the solutions were heated in a 95-100 °C water bath for 10 minutes and then allowed to cool in the water bath for at least 8 hours. The DNA solutions were pipetted into a Nalge Nunc International 96 well optical bottom plate. The 2 x $10^{-4}$ M DODC in 95% ethanol solution was added to achieve a final DODC concentration of 5 x $10^{-6}$ M. Final ethanol concentration was less than 2.5%; ethanol has no absorption in this region. The plate was loaded into a Molecular Devices SpectraMax M5 and absorbance was measured with the samples at 25 °C. Using Molecular Devices SoftMax Pro v5.0.1, absorbance readings were taken at 2 nm intervals from 450 nm to 750 nm. The data was exported as a text file and manipulated using Microsoft Excel.

22mer, 24mer, 15mer, Vet4, VetT4. A sample of 22mer, d(AGGGTTAGGGTTAGGGTTAGGG), was purchased from Integrated DNA Technologies, Inc., Coralville, Iowa. The HPLC purified sample was desalted by ethanol precipitation and stored in PB3 buffer. The concentration was determined from the absorbance at 260 nm with the sample at 293 K in distilled water using an extinction coefficient of 228,500. Stock solutions were prepared in PB3 buffer at concentrations of 1.51 mM, 1 x $10^{-4}$ M, and 4 x $10^{-6}$ M.

A sample of 24mer, d(TTGGGTTAGGGTTAGGGTTAGGGA), was purchased from Integrated DNA Technologies, Inc., Coralville, Iowa. The HPLC purified sample was desalted by ethanol precipitation and stored in PB3 buffer. The concentration was determined from the absorbance at 260 nm with the sample at 293 K in distilled water using an extinction coefficient of 244,300. Stock solutions were prepared in PB3 buffer at concentrations of 2.18 mM, 1 x $10^{-4}$ M, and 4 x $10^{-6}$ M.

A sample of 15mer, d(GGTTGGTGTGGTTGG), was purchased from Integrated DNA Technologies, Inc., Coralville, Iowa. The HPLC purified sample was desalted by ethanol precipitation and stored in PB3 buffer. The concentration was determined from the absorbance at 260 nm with the sample at 293 K in distilled water using an extinction coefficient of 143,300. Stock solutions were prepared in PB3 buffer at concentrations of 2.69 mM, 1 x $10^{-4}$ M, and 4 x $10^{-6}$ M.

A sample of Vet4, d(GGGTTAGGGTTAGGGTTAGGGTTA), was purchased from Integrated DNA Technologies, Inc., Coralville, Iowa. The HPLC purified sample was desalted by ethanol precipitation and stored in PB3 buffer. The concentration was determined from the absorbance at 260 nm with the sample at 293

K in distilled water using an extinction coefficient of 246,300. Stock solutions were prepared in PB3 buffer at concentrations of 2 mM, 1 x $10^{-4}$ M, and 4 x $10^{-6}$ M.

A sample of VetT4, d(TTAGGGTTAGGGTTAGGGTTAGGG), was purchased from Integrated DNA Technologies, Inc., Coralville, Iowa. The HPLC purified sample was desalted by ethanol precipitation and stored in PB3 buffer. The concentration was determined from the absorbance at 260 nm with the sample at 293 K in distilled water using an extinction coefficient of 244,600. Stock solutions were prepared in PB3 buffer at concentrations of 2.87 mM, 1 x $10^{-4}$ M, and 4 x $10^{-6}$ M.

From these stock solutions, DNA samples were prepared at concentrations of 2 x $10^{-8}$, 5 x $10^{-8}$, 1 x $10^{-7}$, 2 x $10^{-7}$, 5 x $10^{-7}$, 1 x $10^{-6}$, 2 x $10^{-6}$, 5 x $10^{-6}$, 1 x $10^{-5}$, 2 x $10^{-5}$, 5 x $10^{-5}$, and 1 x $10^{-4}$ M in PBK buffer. To anneal the DNA the solutions were heated in a 95-100 °C water bath for 10 minutes and then allowed to cool in the water bath for at least 8 hours. The DNA solutions were pipetted into a Nalge Nunc International 96 Well Optical Bottom Plate. The 2 x $10^{-4}$ M DODC in 99.9% DMSO solution was added to achieve a final DODC concentration of 5 x $10^{-6}$ M. Final DMSO concentration was less than 2.5%; DMSO has no absorption in this region. The plate was loaded into a Molecular Devices SpectraMax M5 and absorbance was measured with the samples at 25 °C. Using Molecular Devices SoftMax Pro v5.0.1, absorbance readings were taken at 2 nm intervals from 450 nm to 750 nm. The data was exported as a text file and manipulated using Microsoft Excel. This process was repeated with 2 x $10^{-4}$ M DTDC in 99.9% DMSO solution

Oxy1.5. A sample of Oxy1.5, d(GGGGTTTTGGGG), was purchased from Integrated DNA Technologies, Inc., Coralville, Iowa. The HPLC purified sample was desalted by ethanol precipitation and stored in PB3 buffer. The concentration was determined from the absorbance at 260 nm with the sample at 293 K in distilled water using an extinction coefficient of 115,200. Stock solutions were prepared in PB3 buffer at concentrations of 1.61 mM, $1 \times 10^{-4}$ M, and $4 \times 10^{-6}$ M.

From these stock solutions, DNA samples were prepared at concentrations of $2 \times 10^{-8}$, $5 \times 10^{-8}$, $1 \times 10^{-7}$, $2 \times 10^{-7}$, $5 \times 10^{-7}$, $1 \times 10^{-6}$, $2 \times 10^{-6}$, $5 \times 10^{-6}$, $1 \times 10^{-5}$, $2 \times 10^{-5}$, $5 \times 10^{-5}$, and $1 \times 10^{-4}$ M in PB buffer. To anneal the DNA the solutions were heated in a 95-100 °C water bath for 10 minutes and then allowed to cool in the water bath for at least 8 hours. The DNA solutions were pipetted into a Nalge Nunc International 96 Well Optical Bottom Plate. The $2 \times 10^{-4}$ M DODC in 99.9% DMSO solution was added to achieve a final DODC concentration of $5 \times 10^{-6}$ M. Final DMSO concentration was less than 2.5%; DMSO has no absorption in this region. The plate was loaded into a Molecular Devices SpectraMax M5 and absorbance was measured with the samples at 25 °C. Using Molecular Devices SoftMax Pro v5.0.1, absorbance readings were taken at 2 nm intervals from 450 nm to 750 nm. The data was exported as a text file and manipulated using Microsoft Excel. This process was repeated with $2 \times 10^{-4}$ M DTDC in 99.9% DMSO solution.

Results and Discussion

My research plan is to investigate the similarities and differences in binding of carbocyanine dyes to quadruplex ligands. The interaction between carbocyanine dye and G-quadruplex causes spectrophotometric signatures that are unique and not seen in the binding of carbocyanine dyes to single stranded or duplex DNA. The absorption of the carbocyanine dye is a convenient, sensitive monitor of binding. My investigation aims to establish whether there are differences in dissociation constants and binding modes as well as any other information that the data contains. Plots of absorbance versus wavelength and absorbance versus concentration are used to analyze the data.

DTDC with 22mer. The measured absorbance of 5 x $10^{-6}$ M DTDC is plotted versus wavelength for a series of concentrations of 22mer (Figure 10). The graph

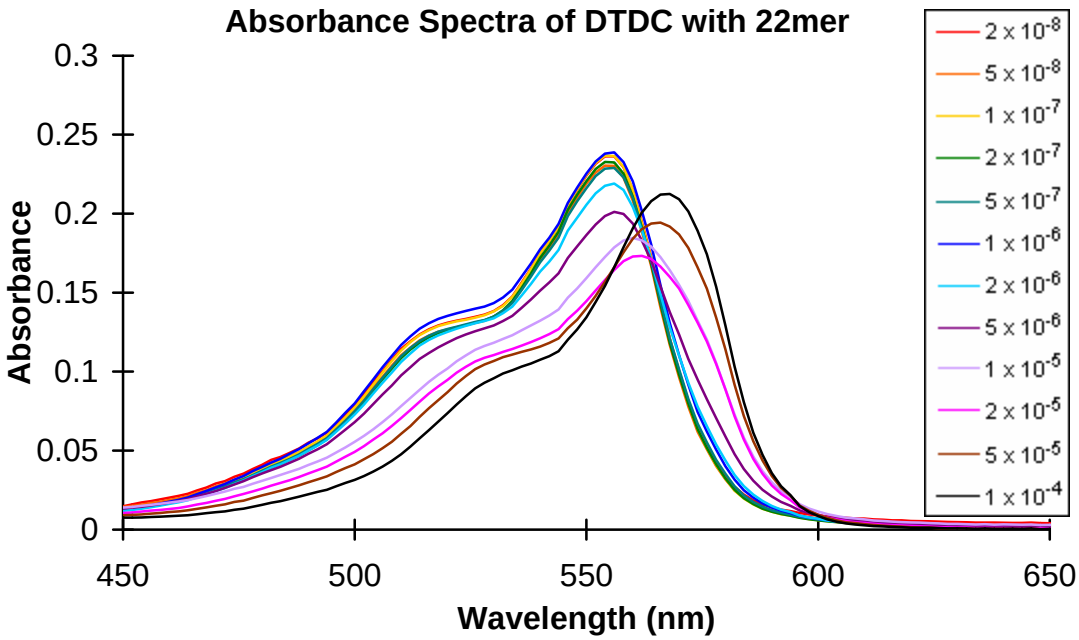


**Figure 10**. Plot of absorbance of 5 x $10^{-6}$ M DTDC with 22mer as a function of wavelength.

shows a decrease in the intensity of $A_{max}$ with increasing DNA concentration up to 2 x $10^{-5}$ M 22mer, after which increasing DNA concentration correlates to an increase in the intensity of $A_{max}$. In addition, increasing DNA concentration appears to cause an increase in the wavelength of $A_{max}$. The spectra show different trends in different wavelength regions, so the measured absorbance of DTDC at 10 nm intervals is plotted as a function of DNA concentration to illustrate these trends (Figure 11). Below 560 nm these plots show an increase in DNA concentration inducing a decrease in maximum absorbance. Above 560 nm an increase in DNA concentration induces an increase in maximum absorbance. The differences in absolute absorbance of these plots make the two groups, above and below 560 nm, difficult to analyze by eye.

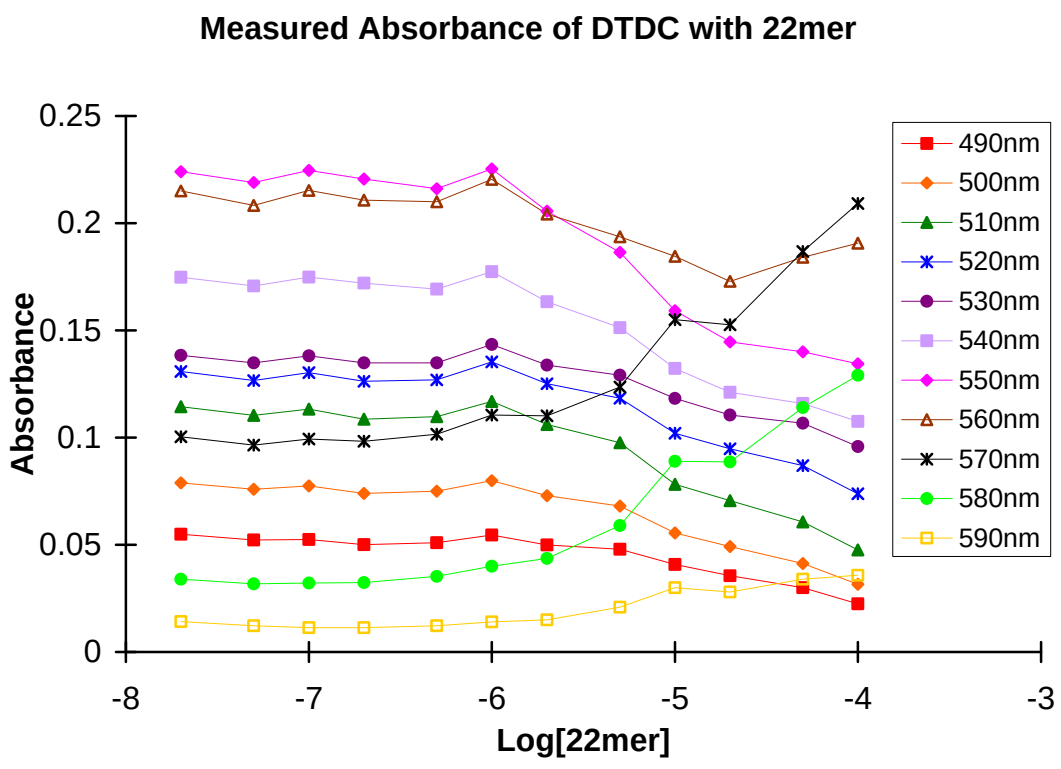


**Figure 11**. Plot of absorbance of DTDC at 5 x $10^{-6}$M as a function of DNA concentration at 10 nm intervals from 490-590 nm.

In order to better compare the different wavelengths, the normalized absorbance, $(A-A_0)/(A_{max}-A_0)$, of DTDC as a function of DNA concentration is plotted for 10 nm intervals from 490 nm to 590 nm (Figure 12). These plots confirm the observation that there is a change in absorption trend at approximately 560 nm.

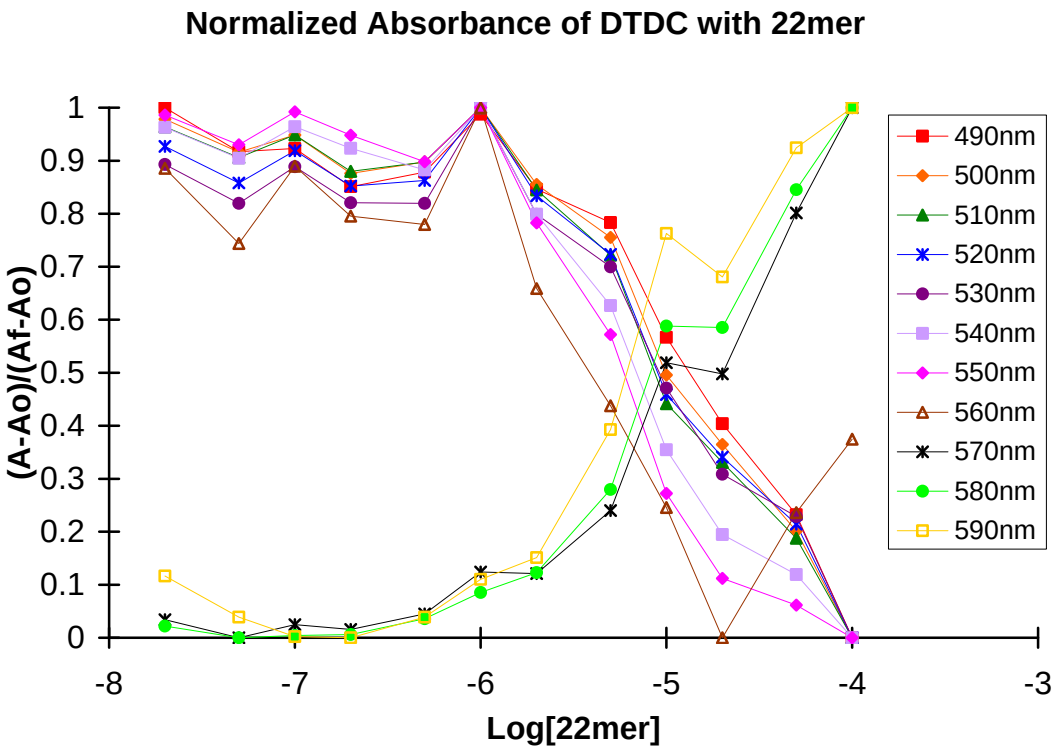


**Figure 12**. Plot of normalized absorbance, $(A-A_0)/(A_{max}-A_0)$, for 5 x $10^{-6}$ M DTDC as a function of DNA concentration. The plots are of the absorbance at 10 nm intervals from 490-590 nm.

To simplify the results further, three wavelengths were selected at which normalized absorbance of DTDC was plotted as a function of 22mer concentration (Figure 13). These wavelengths were selected to represent three different regions of the spectra: the shoulder at approximately 512 nm, the peak of low DNA concentration samples at approximately 552 nm, and the peak of high DNA concentration samples at approximately 576 nm. The results support the model of a single equilibrium for the binding of DTDC with 22mer at approximately 1 x $10^{-5}$ M 22mer.

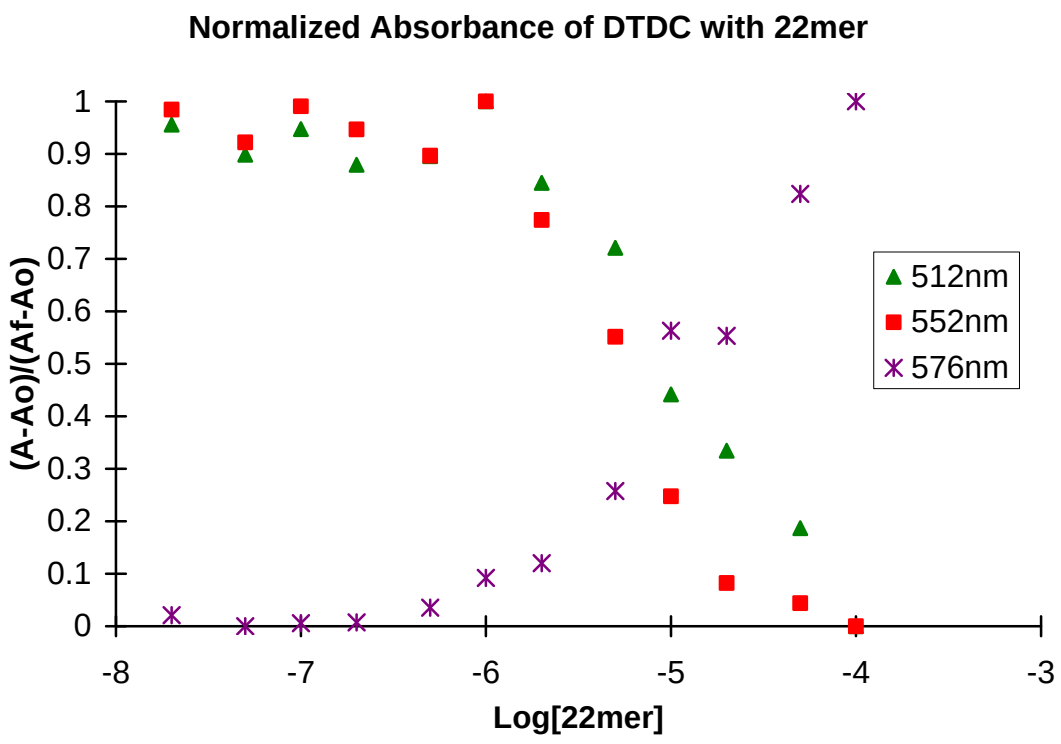


**Figure 13.** Plot of normalized absorbance, $(A-A_0)/(A_{max}-A_0)$, for 5 x $10^{-6}$ M DTDC as a function of DNA concentration. The plots are of the absorbance at the indicated wavelengths.

DTDC with Vet4. The measured absorbance of 5 x $10^{-6}$ M DTDC is plotted versus wavelength for a series of concentrations of Vet4 (Figure 14). Similarly to the case of DTDC with 22mer, the DTDC spectra with Vet4 show a decrease in $A_{max}$ with increasing DNA concentration, but there is not the same increase in $A_{max}$ at the highest DNA concentrations. The DTDC spectra with Vet4 show a similar shift in wavelength of $A_{max}$.

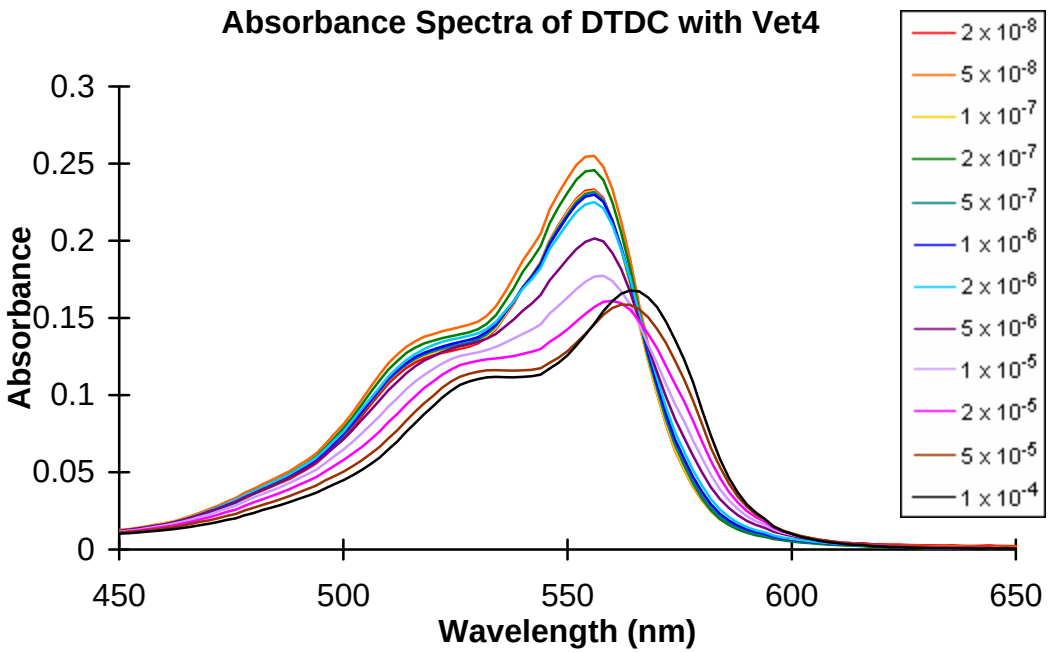


**Figure 14**. Plot of absorbance of 5 x $10^{-6}$ M DTDC with Vet4 as a function of wavelength.

The normalized absorbance of DTDC as a function of Vet4 concentration is plotted for selected wavelengths (Figure 15). The results are similar to the plots for DTDC with 22mer and support the model of a single equilibrium for the binding of DTDC with Vet4 at approximately 1 x $10^{-5}$ M Vet4.

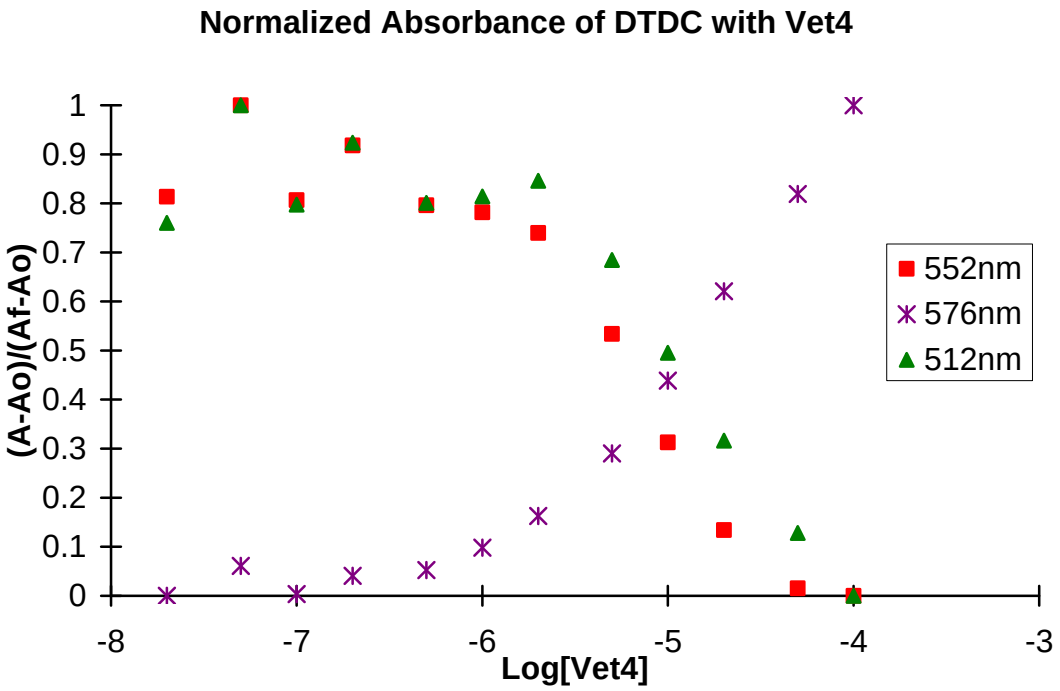


**Figure 15**. Plot of normalized absorbance, $(A-A_0)/(A_{max}-A_0)$, for 5 x $10^{-6}$ M DTDC as a function of DNA concentration. The plots are of the absorbance at the indicated wavelengths.

DTDC with 24mer. The measured absorbance of 5 x $10^{-6}$ M DTDC is plotted versus wavelength for a series of concentrations of 24mer (Figure 16). Similarly to the case of DTDC with 22mer, the DTDC spectra with 24mer show a decrease in $A_{max}$ with increasing DNA concentration, but there is not the same increase in $A_{max}$ at the highest DNA concentrations. The DTDC spectra with Vet4 show a similar shift in wavelength of $A_{max}$.

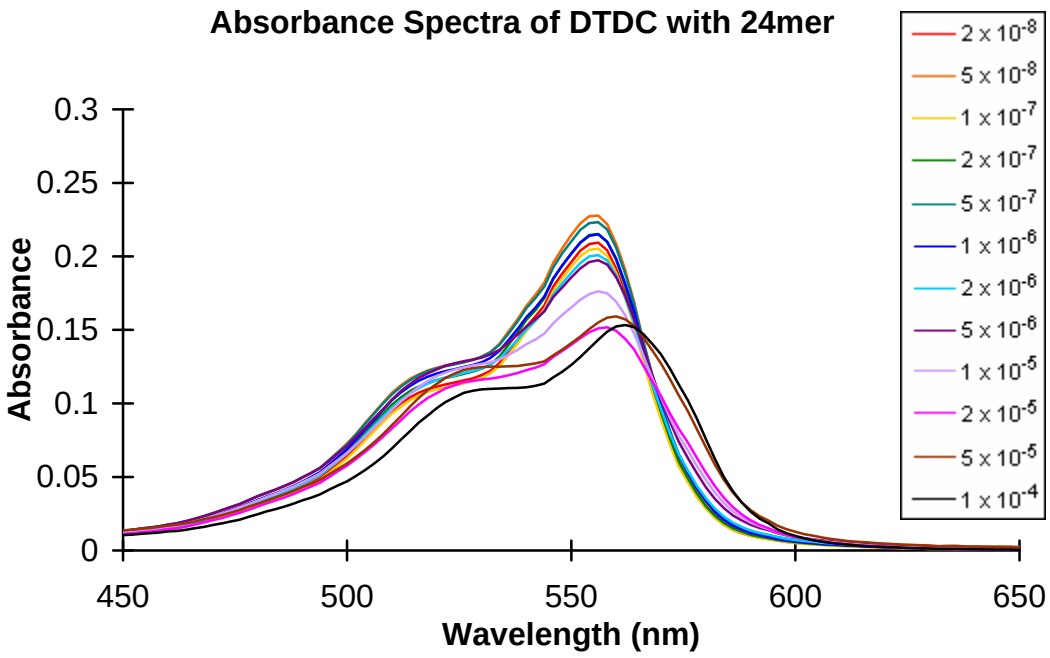


**Figure 16**. Plot of absorbance of 5 x $10^{-6}$ M DTDC with 24mer as a function of wavelength.

The normalized absorbance of DTDC as a function of 24mer concentration is plotted for selected wavelengths (Figure 17). The results are similar to the plots for DTDC with 22mer and support the model of a single equilibrium for the binding of DTDC with 24mer between 1 x $10^{-5}$ M and 2 x $10^{-5}$ M 24mer.

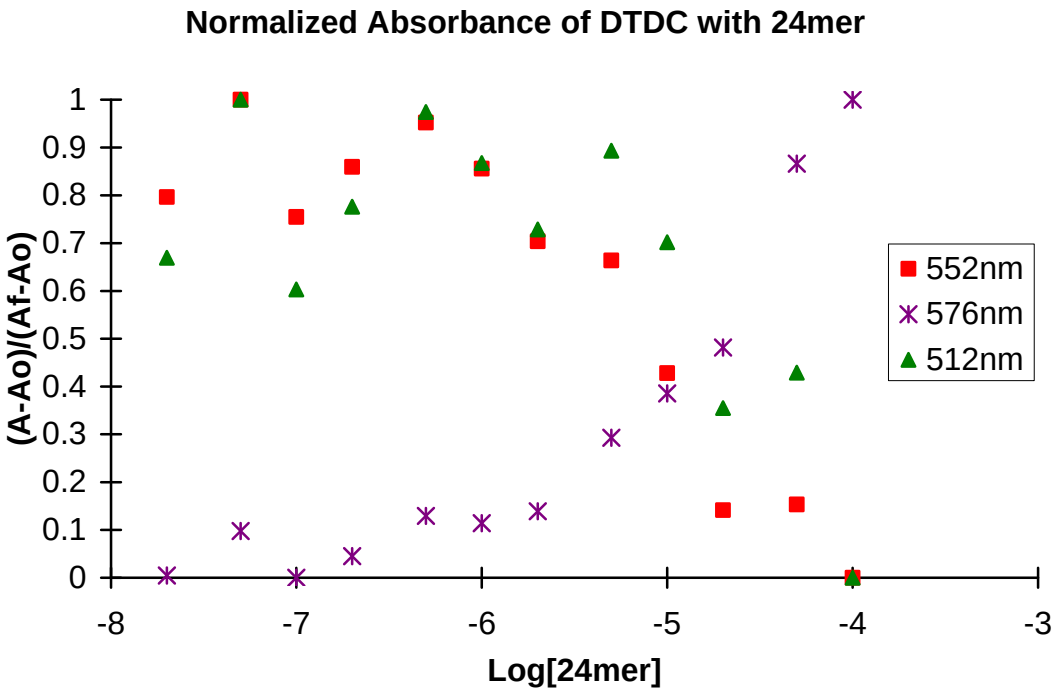


**Figure 17.** Plot of normalized absorbance, $(A-A_0)/(A_{max}-A_0)$, for 5 x $10^{-6}$ M DTDC as a function of DNA concentration. The plots are of the absorbance at the indicated wavelengths.

DTDC with 15mer. The measured absorbance of 5 x $10^{-6}$ M DTDC is plotted versus wavelength for a series of concentrations of 15mer (Figure 18). Similarly to the case of DTDC with 22mer, the DTDC spectra with 15mer show a decrease in $A_{max}$ with increasing DNA concentration, but there is not the same increase in $A_{max}$ at the highest DNA concentrations. The DTDC with 15mer spectra show a similar shift in wavelength of $A_{max}$.

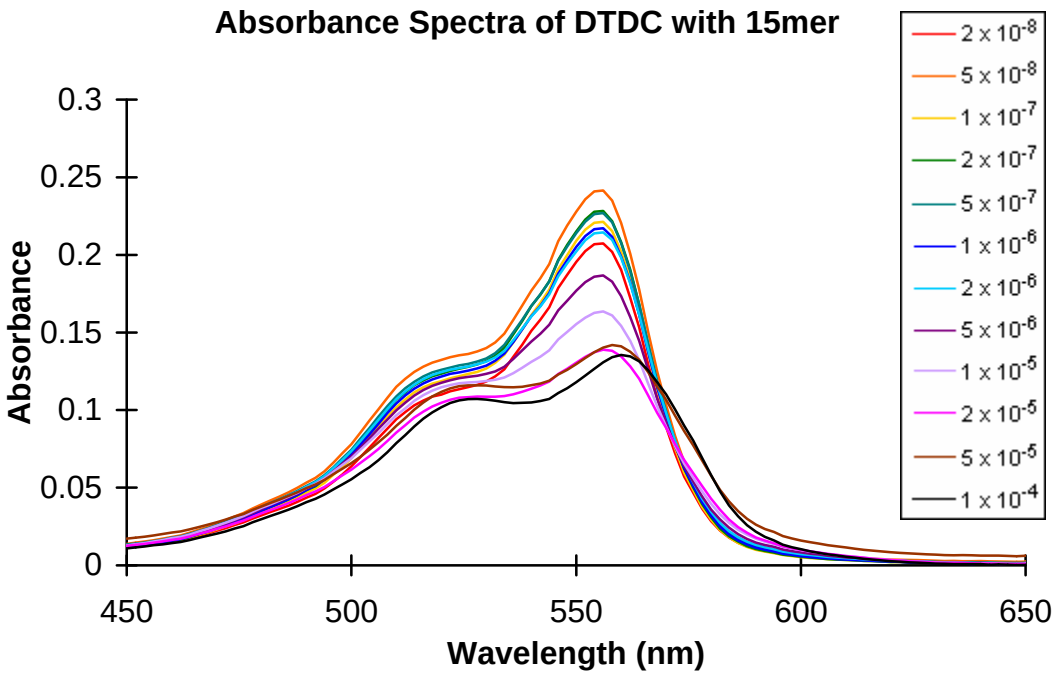


**Figure 18**. Plot of absorbance of 5 x $10^{-6}$ M DTDC with 15mer as a function of wavelength.

The normalized absorbance of DTDC as a function of 15mer concentration is plotted for selected wavelengths (Figure 19). The results are similar to the plots for DTDC with 22mer and support the model of a single equilibrium for the binding of DTDC with 15mer at approximately 1 x $10^{-5}$ M 15mer.

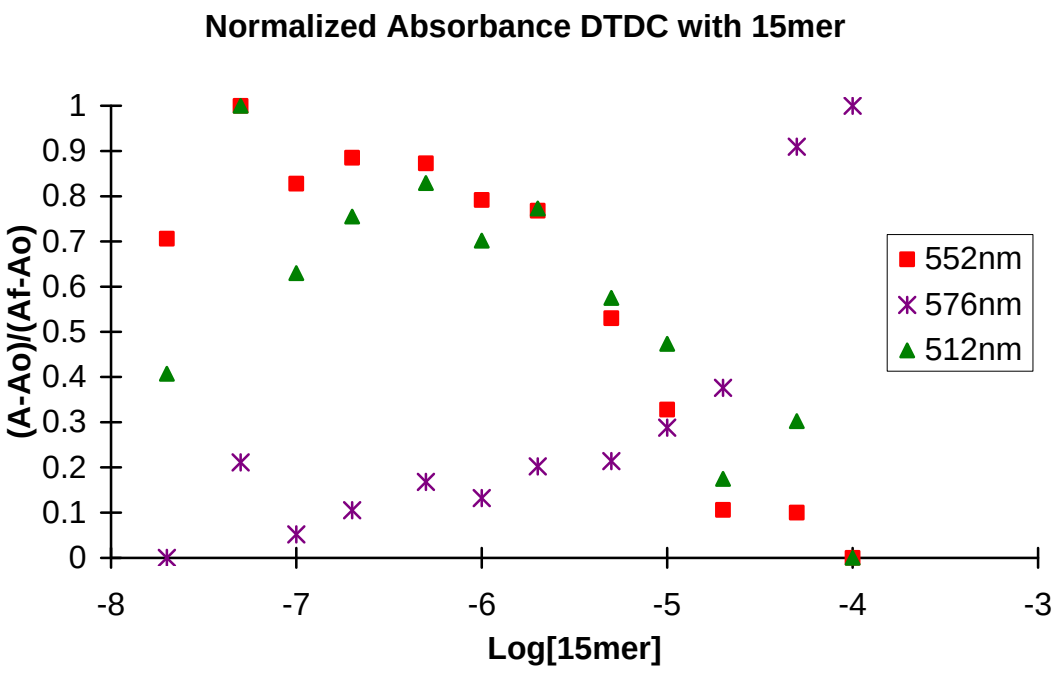


**Figure 19**. Plot of normalized absorbance, $(A-A_0)/(A_{max}-A_0)$, for 5 x $10^{-6}$ M DTDC as a function of DNA concentration. The plots are of the absorbance at the indicated wavelengths.

DTDC with VetT4. The measured absorbance of 5 x $10^{-6}$ M DTDC is plotted versus wavelength for a series of concentrations of VetT4 (Figure 20). Similarly to the case of DTDC with 22mer, the DTDC spectra with VetT4 show a decrease in $A_{max}$ with increasing DNA concentration followed by an increase in $A_{max}$ at the highest concentrations. The DTDC spectra with Vet4 show a similar shift in wavelength of $A_{max}$.

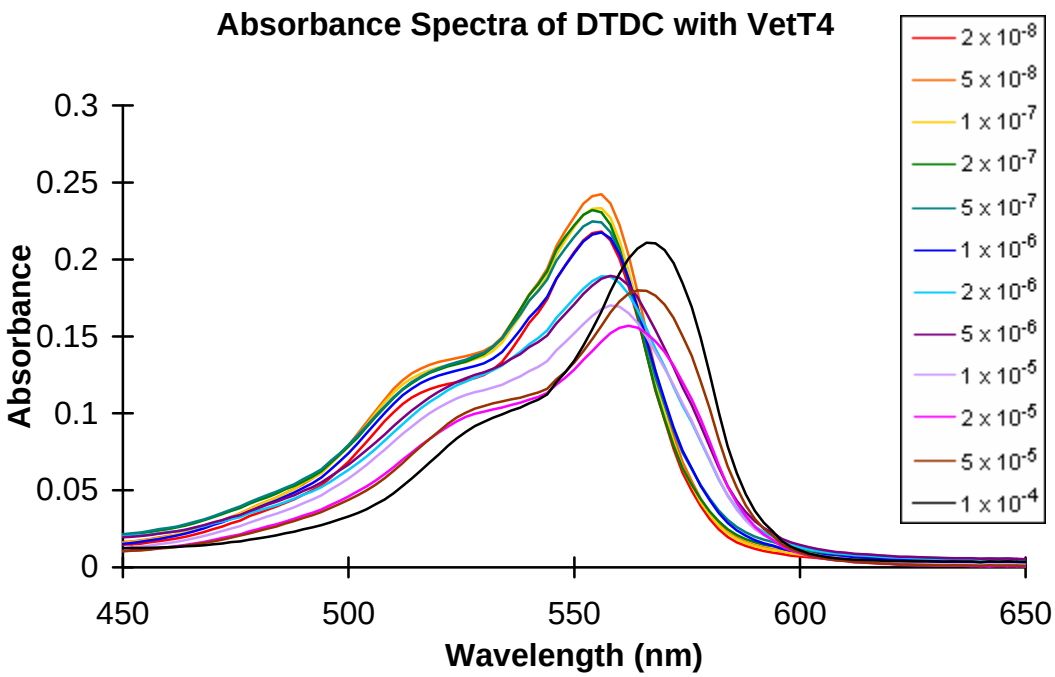


**Figure 20**. Plot of absorbance of 5 x $10^{-6}$ M DTDC with VetT4 as a function of wavelength.

The normalized absorbance of DTDC as a function of VetT4 concentration is plotted for selected wavelengths (Figure 21). The results are similar to the plots for DTDC with 22mer and support the model of a single equilibrium for the binding of DTDC with VetT4 between 2 x $10^{-6}$ M and 1 x $10^{-5}$ M VetT4.

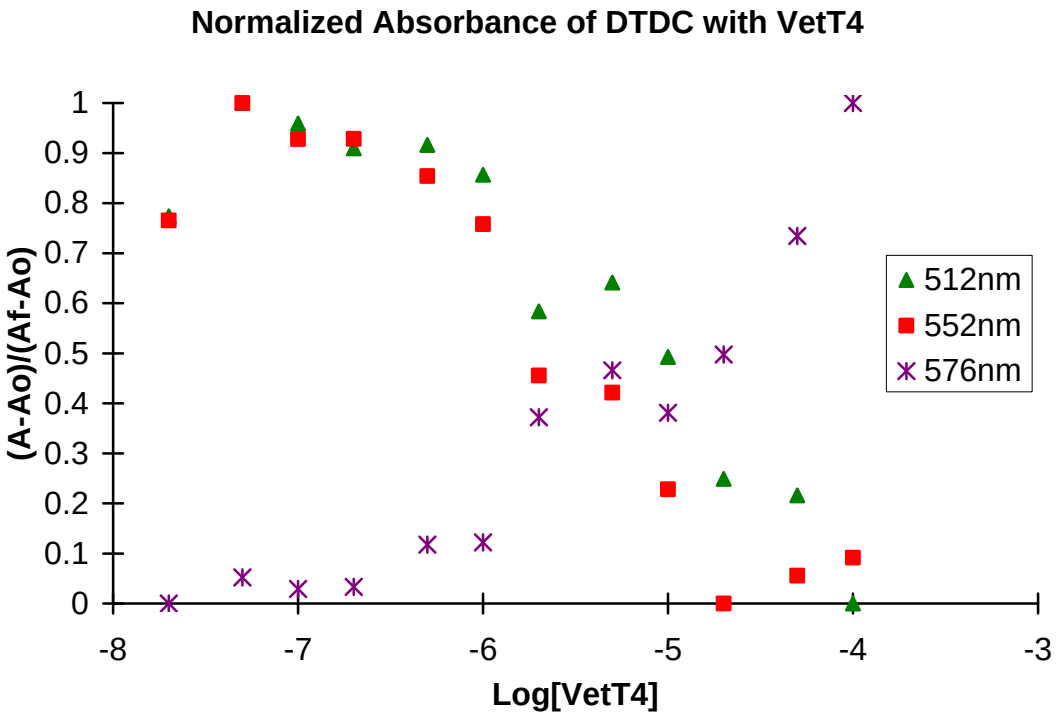


**Figure 21**. Plot of normalized absorbance, $(A-A_0)/(A_{max}-A_0)$, for 5 x $10^{-6}$ M DTDC as a function of DNA concentration. The plots are of the absorbance at the indicated wavelengths.

DTDC with Oxy1.5. The measured absorbance of 5 x $10^{-6}$ M DTDC is plotted versus wavelength for a series of concentrations of Oxy1.5 (Figure 22). Similarly to the case of DTDC with 22mer, the DTDC spectra with Oxy1.5 show a decrease in $A_{max}$ with increasing DNA concentration, but this decreasing trend continues through the highest DNA concentrations. The DTDC spectra with Oxy1.5 show no shift in the wavelength of $A_{max}$.

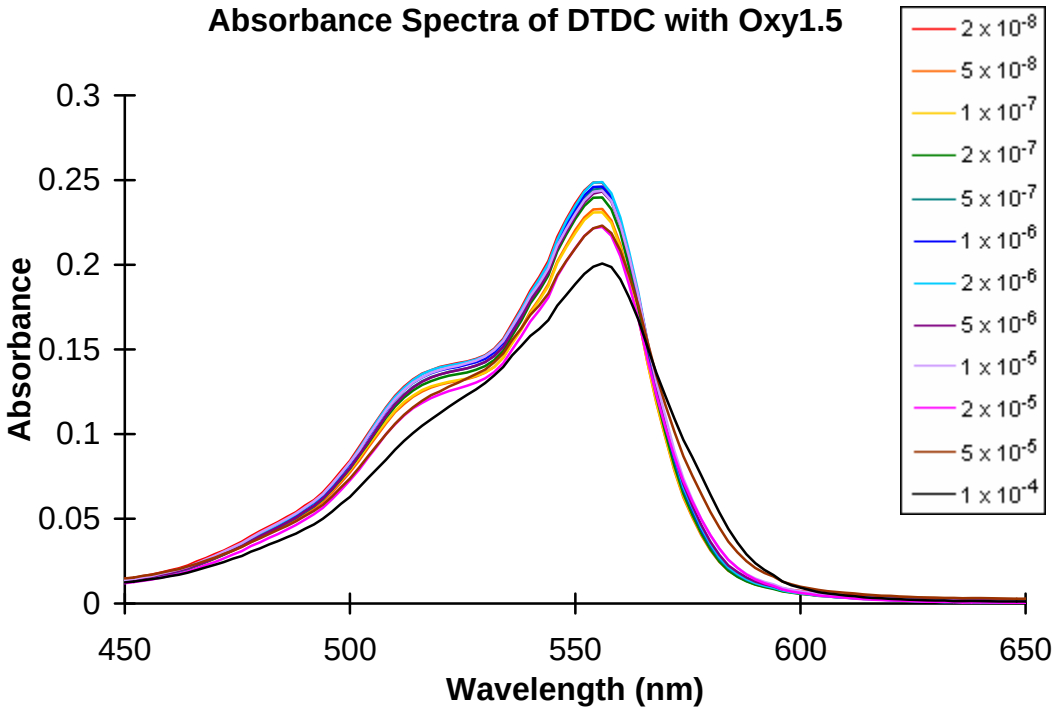


**Figure 22**. Plot of absorbance of 5 x $10^{-6}$ M DTDC with Oxy1.5 as a function of wavelength.

The normalized absorbance of DTDC as a function of Oxy1.5 concentration is plotted for selected wavelengths (Figure 23). The results are similar to the plots for DTDC with 22mer and support the model of a single equilibrium for the binding of DTDC with Oxy1.5 between 2 x $10^{-5}$ M and 5 x $10^{-5}$ M Oxy1.5.

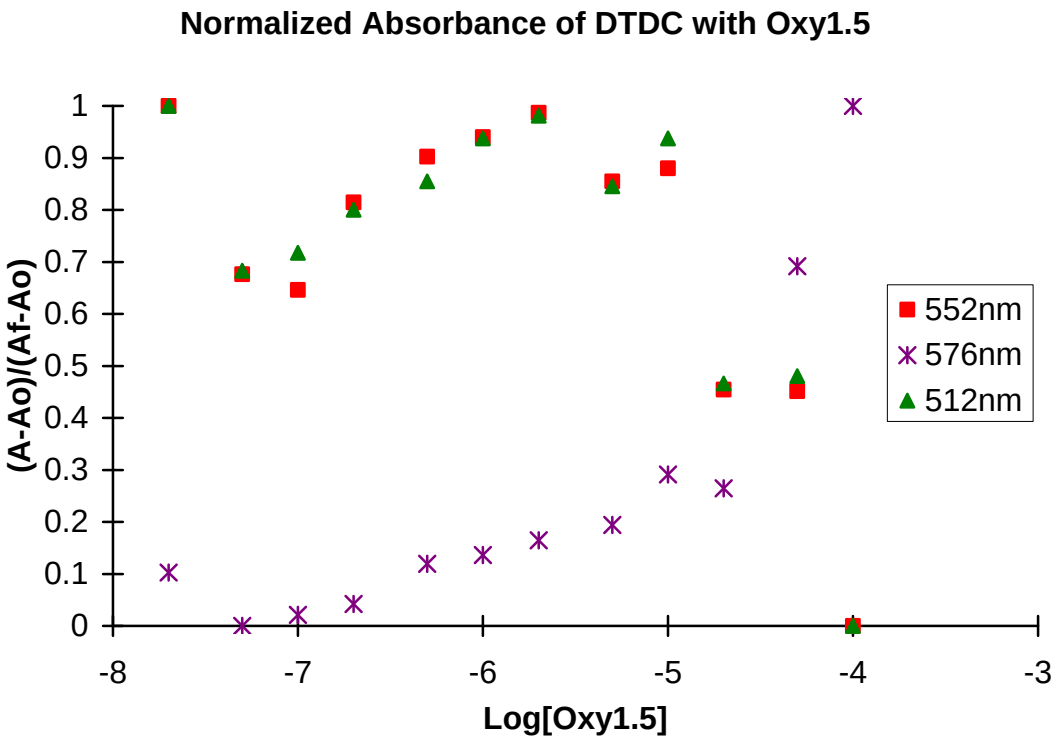


**Figure 23**. Plot of normalized absorbance, $(A-A_0)/(A_{max}-A_0)$, for 5 x $10^{-6}$ M DTDC as a function of DNA concentration. The plots are of the absorbance at the indicated wavelengths.

<u>DODC with 22mer.</u> The measured absorbance of 5 x $10^{-6}$ M DODC is plotted versus wavelength for a series of concentrations of 22mer (Figure 24). The plots show a decrease in the intensity of $A_{max}$ with increasing DNA concentration up to 5 x $10^{-5}$ M 22mer, after which point the intensity of $A_{max}$ remains approximately constant with increasing DNA concentration. Also, the plots show an increase in the wavelength of $A_{max}$ with an increase in DNA concentration.

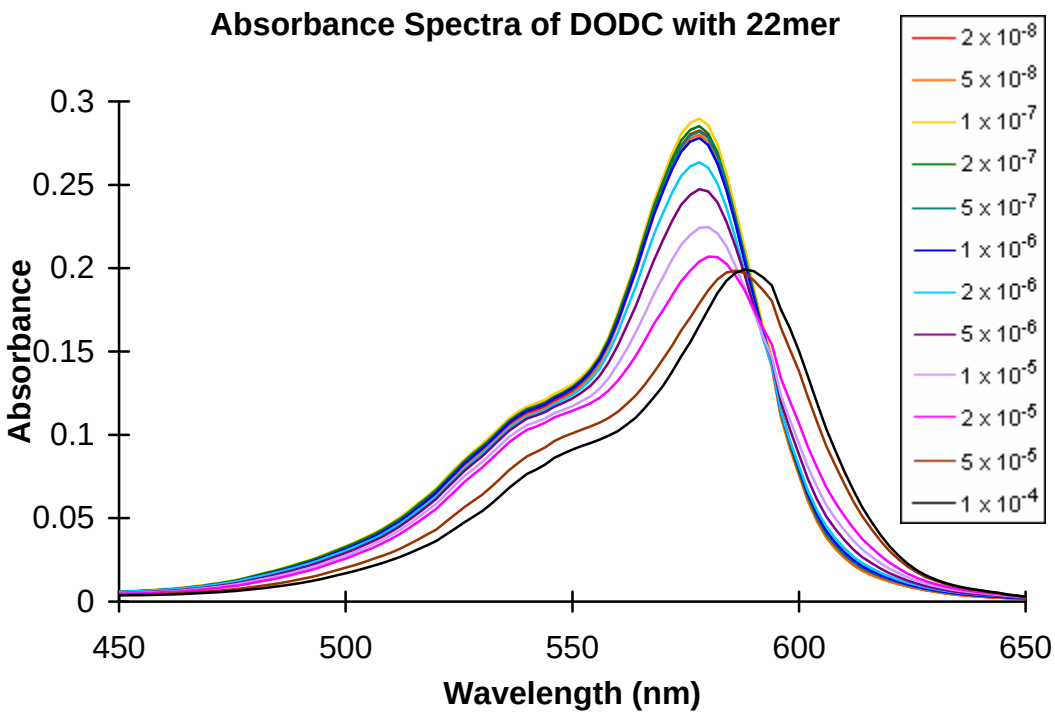


**Figure 24**. Plot of absorbance of 5 x $10^{-6}$ M DODC with 22mer as a function of wavelength. Spectra were renormalized to 50%.

The normalized absorbance of DODC as a function of 22mer concentration is plotted for selected wavelengths (Figure 25). The results support the model of a single equilibrium for the binding of DODC with 22mer between 1 x $10^{-5}$ M and 2 x $10^{-5}$ M 22mer.

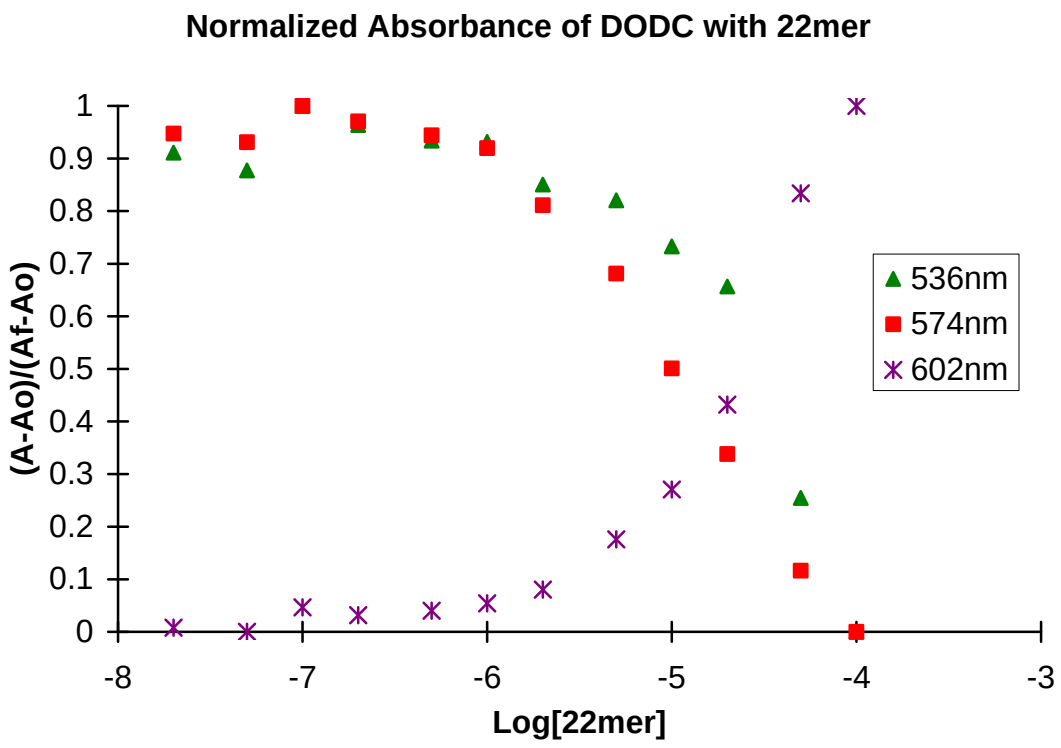


**Figure 25**. Plot of normalized absorbance, $(A-A_0)/(A_{max}-A_0)$, for 5 x $10^{-6}$ M DODC as a function of DNA concentration. The plots are of the absorbance at the indicated wavelengths.

DODC with Vet4. The measured absorbance of 5 x $10^{-6}$ M DODC is plotted versus wavelength for a series of concentrations of Vet4 (Figure 26). Similarly to the case of DODC with 22mer, the DODC spectra with Vet4 show a decrease in $A_{max}$ with increasing DNA concentration. However, the DODC spectra with Vet4 show an increase in $A_{max}$ at the highest concentration that is not present in the DODC spectra with 22mer. The DODC spectra with Vet4 show a similar shift in the wavelength of $A_{max}$.

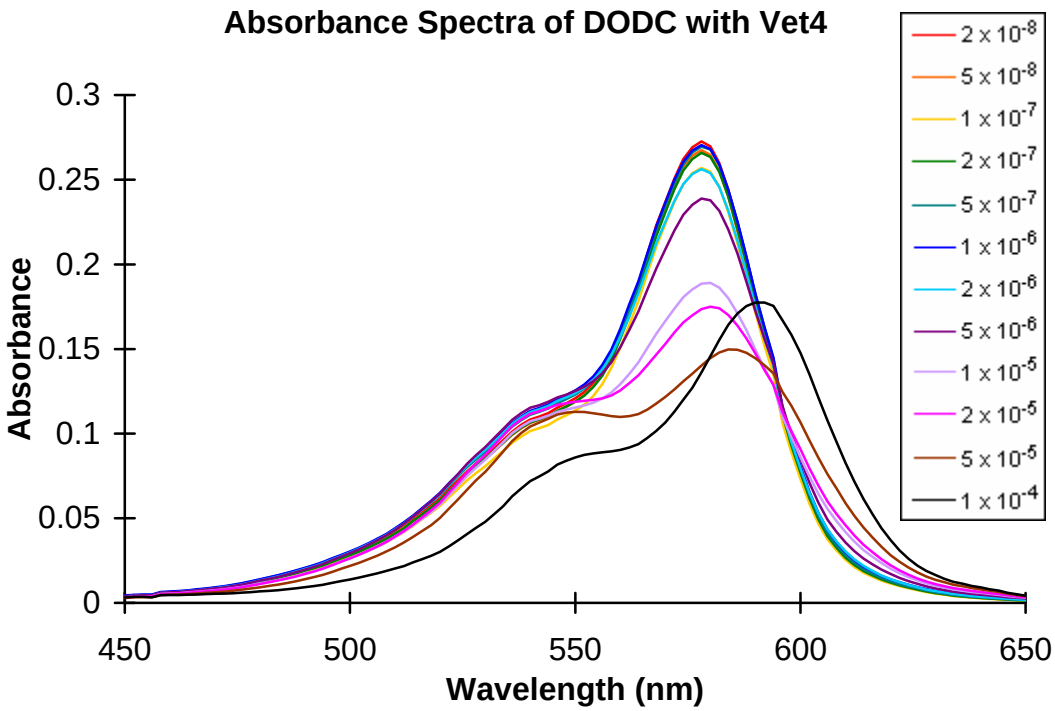


**Figure 26**. Plot of absorbance of 5 x $10^{-6}$ M DODC with Vet4 as a function of wavelength. Spectra were renormalized to 50%.

The normalized absorbance of DODC as a function of Vet4 concentration is plotted for selected wavelengths (Figure 27). The results are similar to the plots for DODC with 22mer and support the model of a single equilibrium for the binding of DODC with Vet4 between 1 x $10^{-5}$ M and 5 x $10^{-5}$ M Vet4.

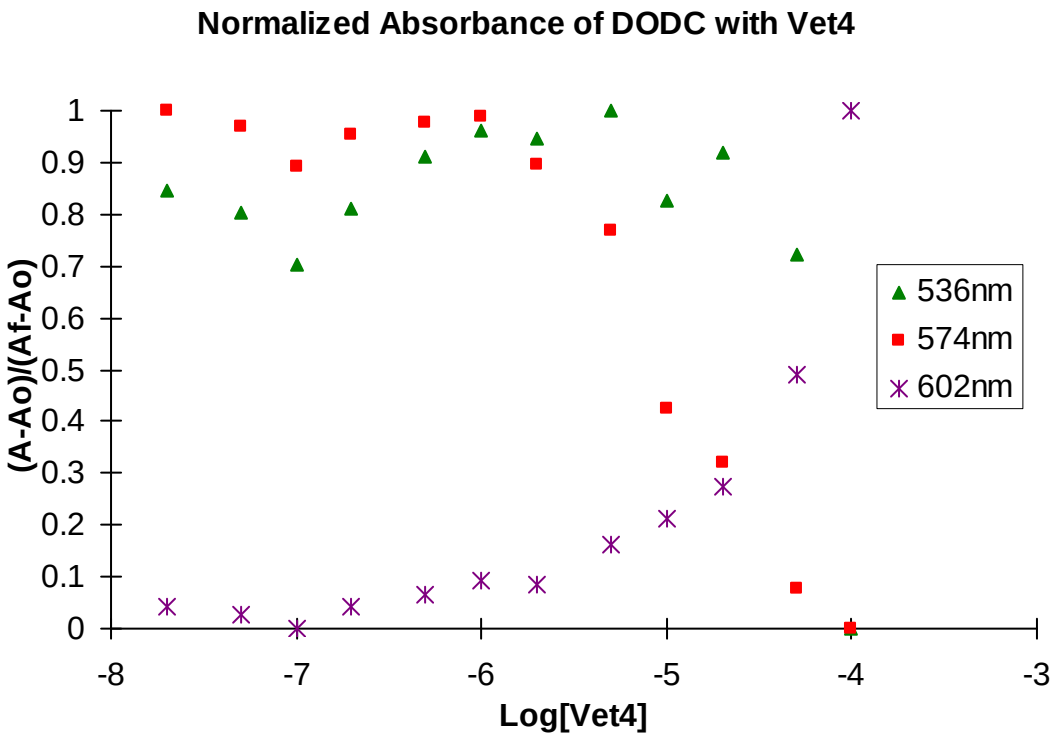


**Figure 27**. Plot of normalized absorbance, $(A-A_0)/(A_{max}-A_0)$, for 5 x $10^{-6}$ M DODC as a function of DNA concentration. The plots are of the absorbance at the indicated wavelengths.

DODC with 24mer. The measured absorbance of 5 x $10^{-6}$ M DODC is plotted versus wavelength for a series of concentrations of 24mer (Figure 28). Similarly to the case of DODC with 22mer, the DODC spectra with 24mer show a decrease in $A_{max}$ with increasing DNA concentration, but this decreasing trend continues to the highest concentrations. The DODC spectra with 24mer show a similar shift in the wavelength of $A_{max}$.

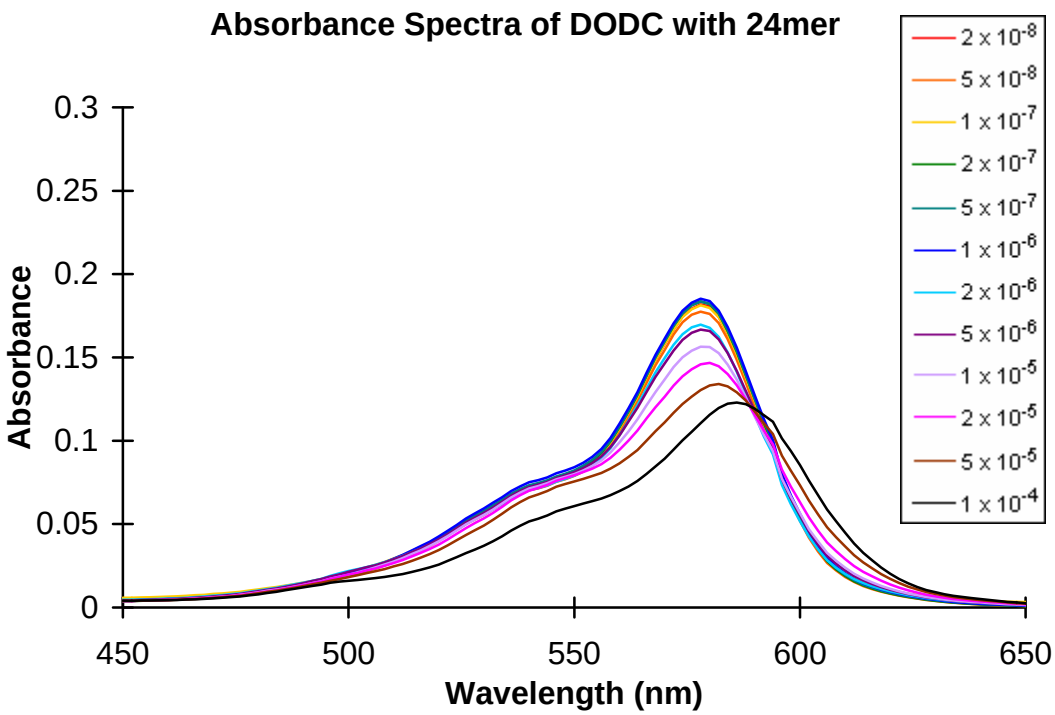


**Figure 28**. Plot of absorbance of 5 x $10^{-6}$ M DODC with 24mer as a function of wavelength. Spectra were renormalized to 50%.

The normalized absorbance of DODC as a function of 24mer concentration is plotted for selected wavelengths (Figure 29). The results are similar to the plots for DODC with 22mer and support the model of a single equilibrium for the binding of DODC with 24mer between 2 x $10^{-5}$ M and 5 x $10^{-5}$ M 24mer.

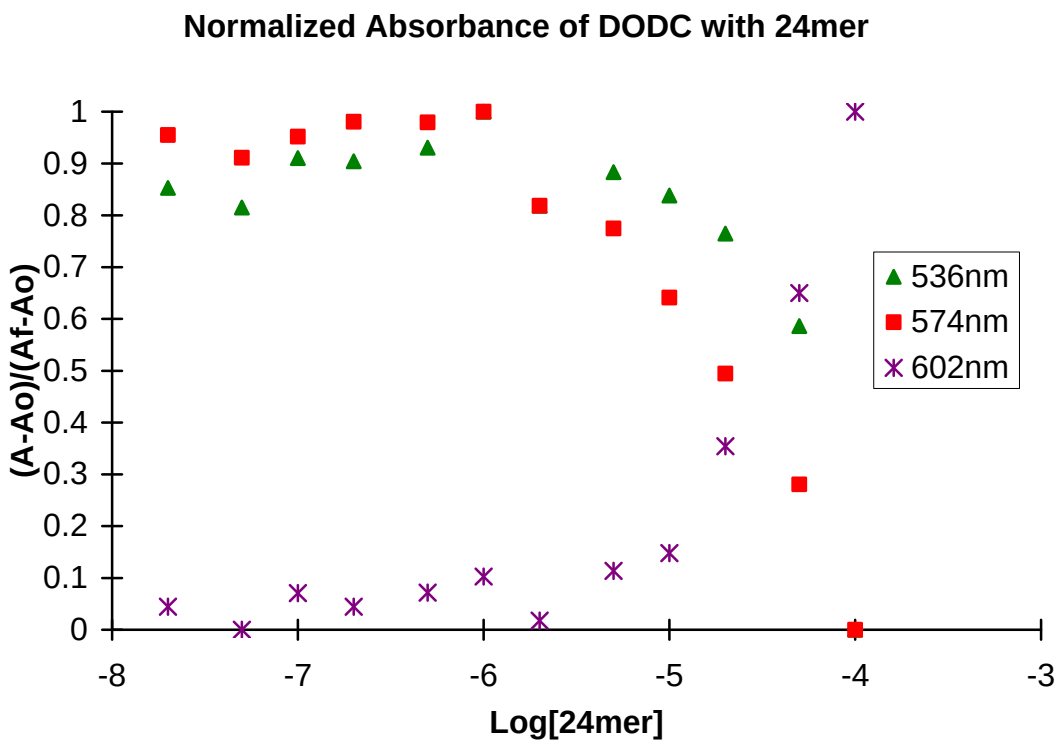


**Figure 29**. Plot of normalized absorbance, $(A-A_0)/(A_{max}-A_0)$, for 5 x $10^{-6}$ M DODC as a function of DNA concentration. The plots are of the absorbance at the indicated wavelengths.

DODC with 15mer. The measured absorbance of 5 x $10^{-6}$ M DODC is plotted versus wavelength for a series of concentrations of 15mer (Figure 30). Similarly to the case of DODC with 22mer, the DODC spectra with15mer show a decrease in $A_{max}$ with increasing DNA concentration and approximate consistency at the highest concentrations. The DODC spectra with 15mer show a similar shift in the wavelength of $A_{max}$.

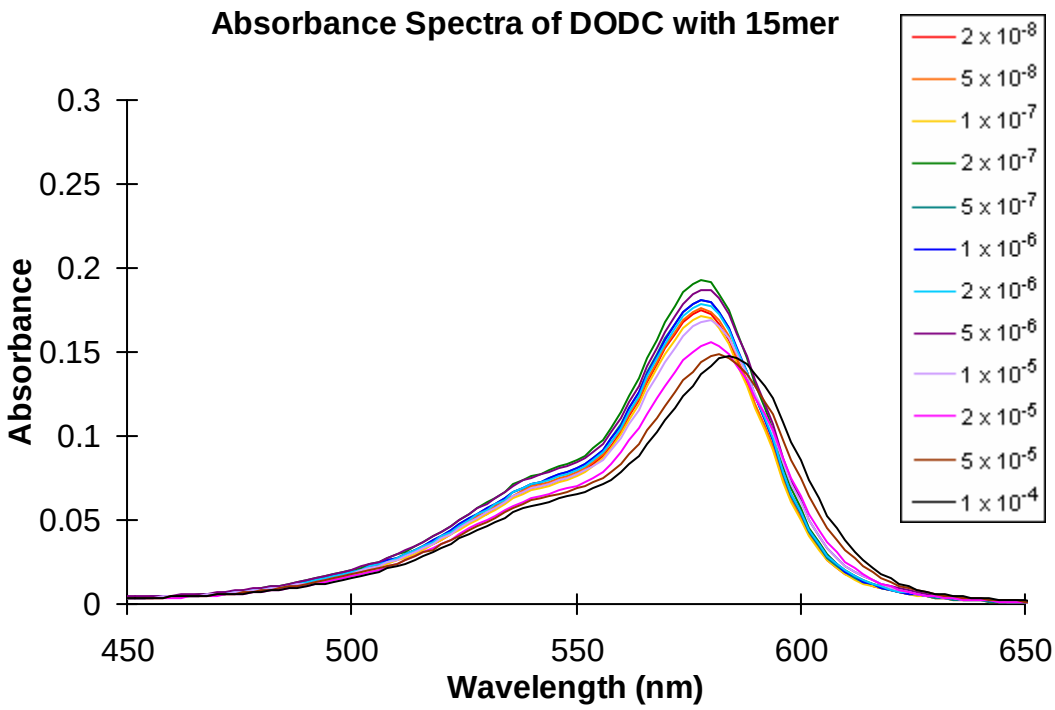


**Figure 30**. Plot of absorbance of 5 x $10^{-6}$ M DODC with 15mer as a function of wavelength. Spectra were renormalized to 50%.

The normalized absorbance of DODC as a function of 15mer concentration is plotted for selected wavelengths (Figure 31). The results are similar to the plots for DODC with 22mer and support the model of a single equilibrium for the binding of DODC with 15mer between 1 x $10^{-5}$ M and 2 x $10^{-5}$ M 15mer.

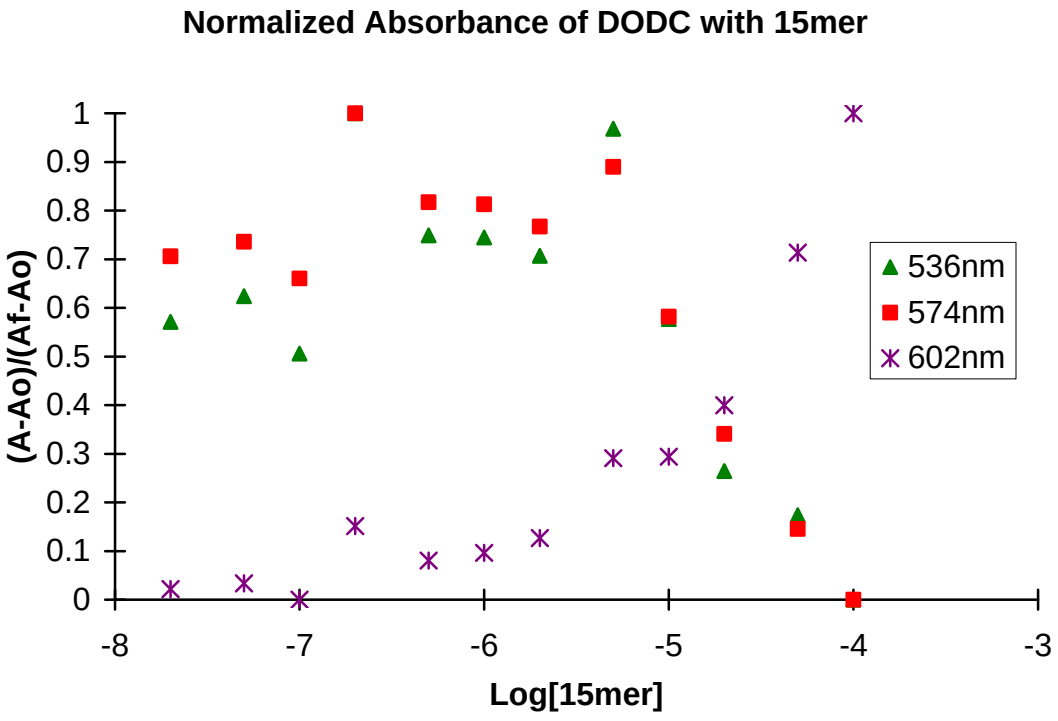


**Figure 31**. Plot of normalized absorbance, $(A-A_0)/(A_{max}-A_0)$, for 5 x $10^{-6}$ M DODC as a function of DNA concentration. The plots are of the absorbance at the indicated wavelengths.

<u>DODC with VetT4.</u> The measured absorbance of 5 x $10^{-6}$ M DODC is plotted versus wavelength for a series of concentrations of VetT4 (Figure 32). Similarly to the case of DODC with 22mer, the DODC spectra with VetT4 show a decrease in $A_{max}$ with increasing DNA concentration, but the consistency of $A_{max}$ at the highest concentrations includes the 2 x $10^{-5}$ M DNA sample. The DODC spectra with VetT4 show a similar shift in the wavelength of $A_{max}$.

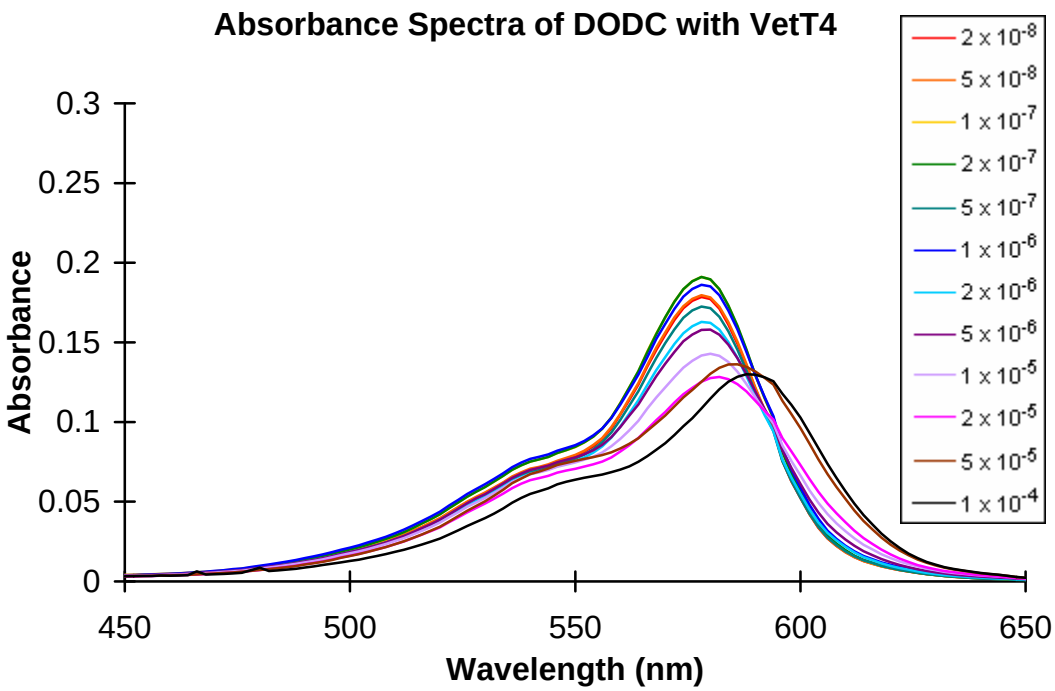


**Figure 32**. Plot of absorbance of 5 x $10^{-6}$ M DODC with VetT4 as a function of wavelength. Spectra were renormalized to 50%.

The normalized absorbance of DODC as a function of VetT4 concentration is plotted for selected wavelengths (Figure 33). The results are similar to the plots for DODC with 22mer and support the model of a single equilibrium for the binding of DODC with VetT4 between 1 x $10^{-5}$ M and 2 x $10^{-5}$ M VetT4.

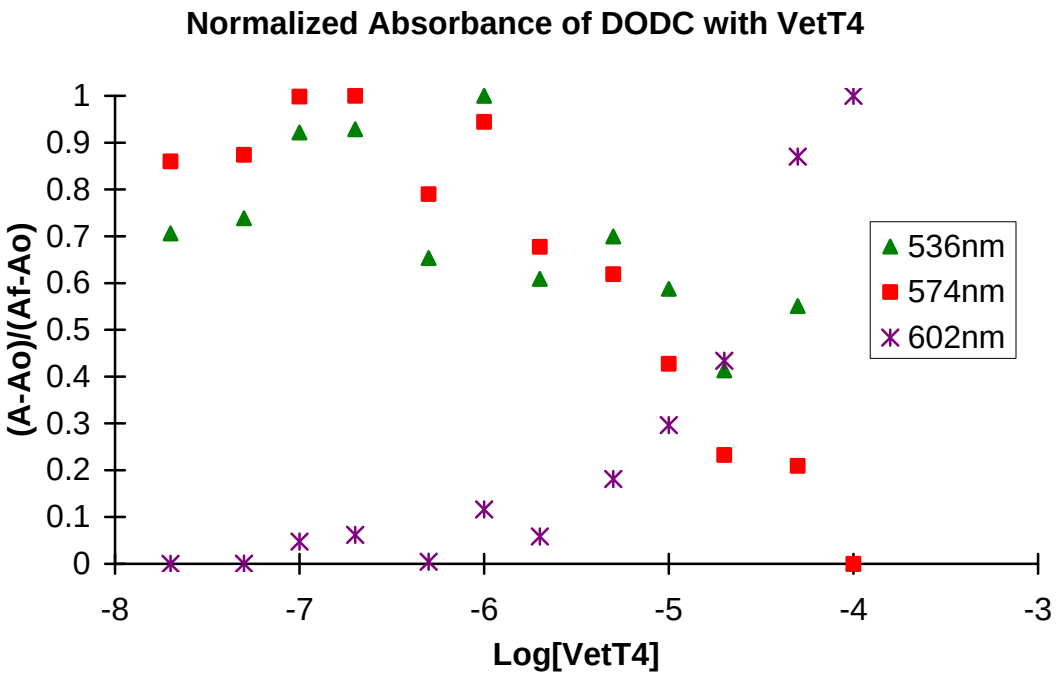


**Figure 33**. Plot of normalized absorbance, $(A-A_0)/(A_{max}-A_0)$, for 5 x $10^{-6}$ M DODC as a function of DNA concentration. The plots are of the absorbance at the indicated wavelengths.

DODC with Oxy1.5. The measured absorbance of 5 x $10^{-6}$ M DODC is plotted versus wavelength for a series of concentrations of Oxy1.5 (Figure 34). Similarly to the case of DODC with 22mer, the DODC spectra with Oxy1.5 show a decrease in $A_{max}$ with increasing DNA concentration, but this decreasing trend continues through the highest DNA concentrations. The DODC spectra with Oxy1.5 do not show a shift in the wavelength of $A_{max}$.

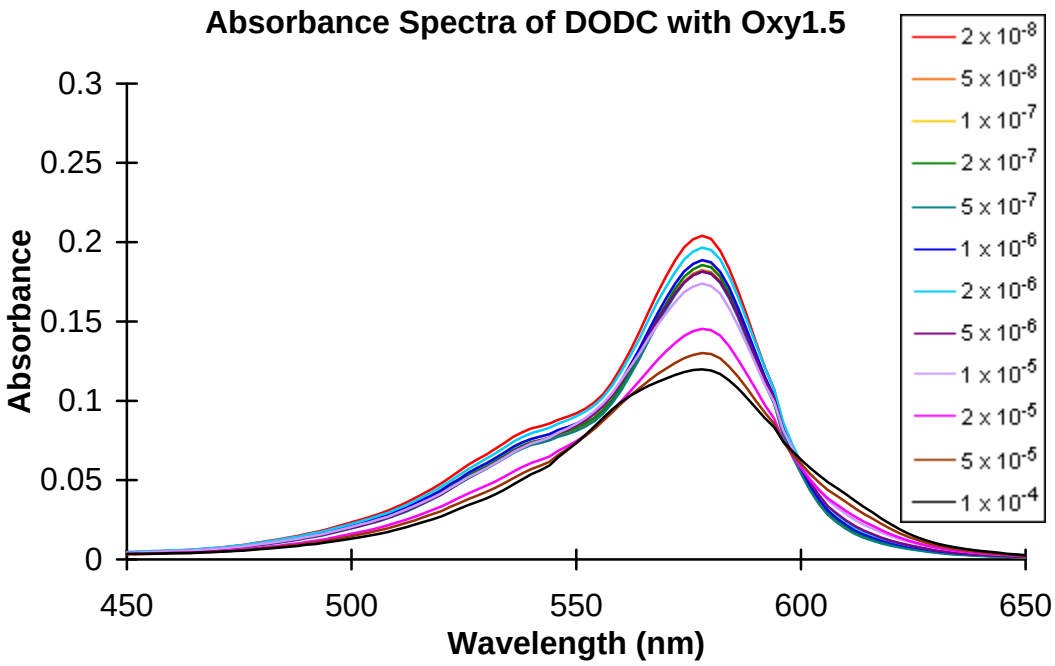


**Figure 34**. Plot of absorbance of 5 x $10^{-6}$ M DODC with Oxy1.5 as a function of wavelength. Spectra were renormalized to 50%.

The normalized absorbance of DODC as a function of Oxy1.5 concentration is plotted for selected wavelengths (Figure 35). The results are similar to the plots for DODC with 22mer and support the model of a single equilibrium for the binding of DODC with Oxy1.5 at approximately 1 x $10^{-5}$ M Oxy1.5.

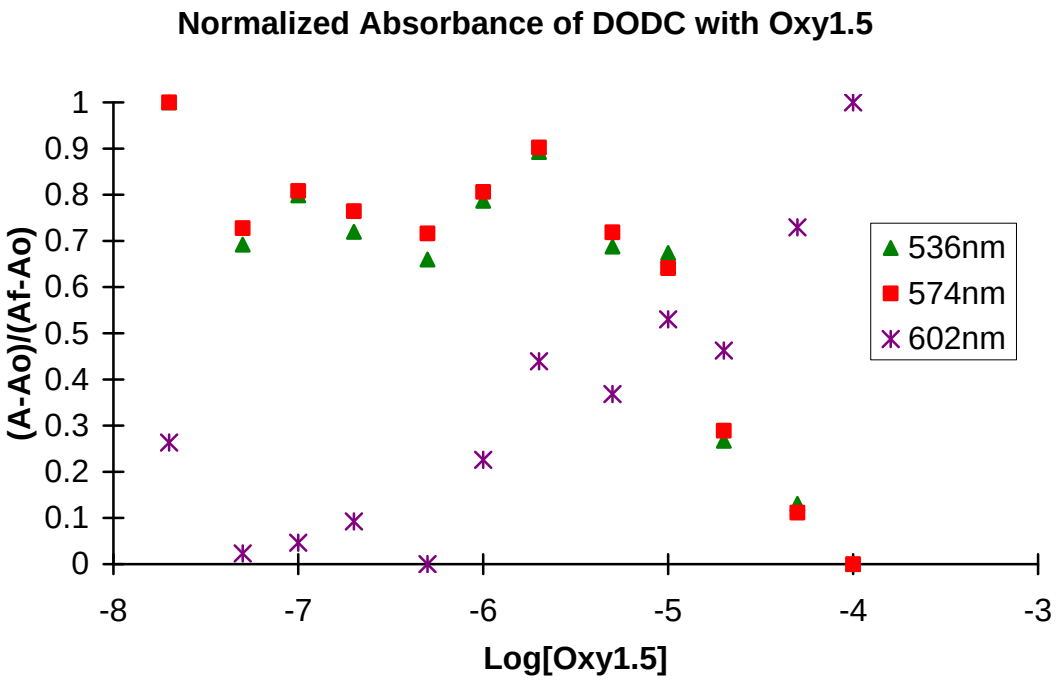


**Figure 35**. Plot of normalized absorbance, $(A-A_0)/(A_{max}-A_0)$, for 5 x $10^{-6}$ M DODC as a function of DNA concentration. The plots are of the absorbance at the indicated wavelengths.

DODC with VetU6. The measured absorbance of 5 x $10^{-6}$ M DODC is plotted versus wavelength for a series of concentrations of VetU6 (Figure 36). Similarly to the case of DODC with 22mer, the DODC spectra with VetU6 show a decrease in $A_{max}$ with increasing DNA concentration and approximate consistency at the highest concentrations. The DODC spectra with VetU6 show a similar shift in the wavelength of $A_{max}$.

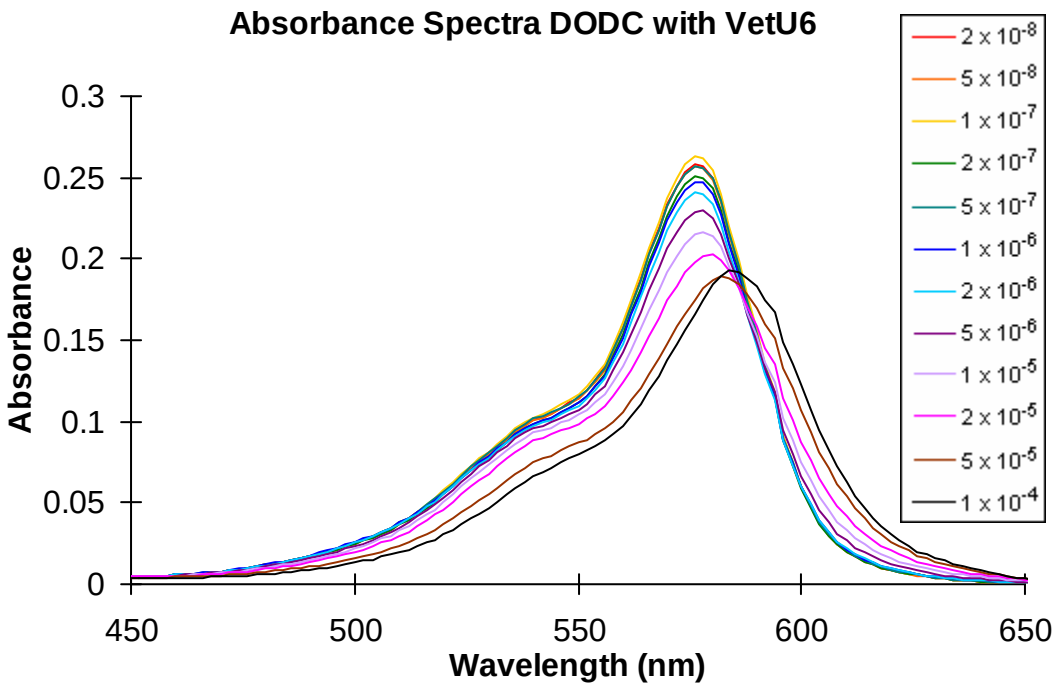


**Figure 36**. Plot of absorbance of 5 x $10^{-6}$ M DODC with VetU6 as a function of wavelength. Spectra were renormalized to 33%.

The normalized absorbance of DODC as a function of VetU6 concentration is plotted for selected wavelengths (Figure 37). The results are similar to the plots for DODC with 22mer and support the model of a single equilibrium for the binding of DODC with VetU6 between 1 x $10^{-5}$ M and 2 x $10^{-5}$ M VetU6.

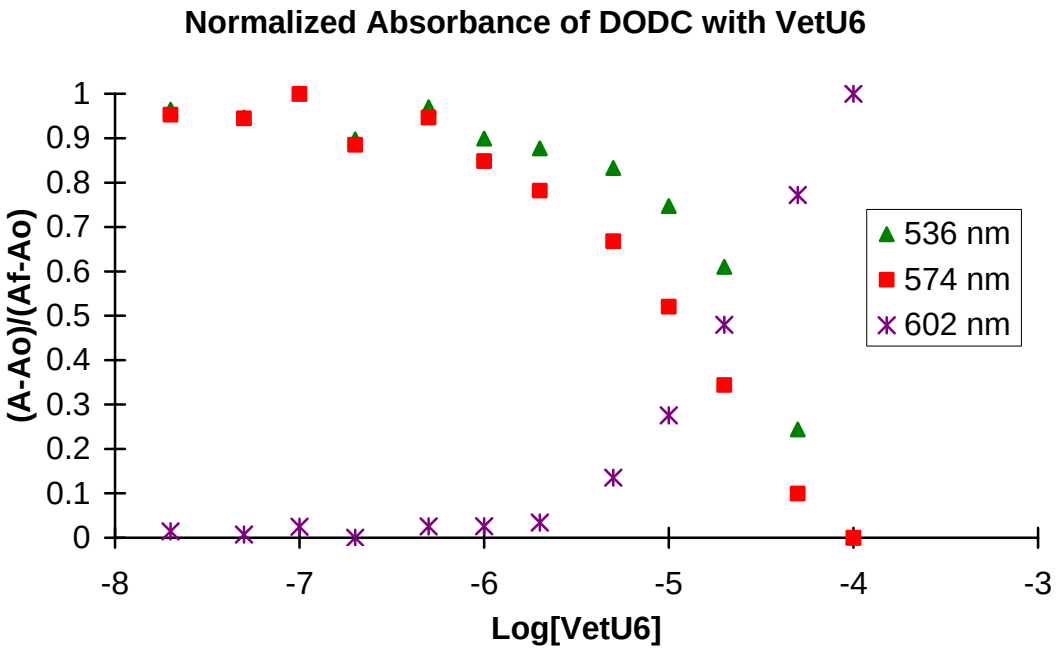


**Figure 37**. Plot of normalized absorbance, $(A-A_0)/(A_{max}-A_0)$, for 5 x $10^{-6}$ M DODC as a function of DNA concentration. The plots are of the absorbance at the indicated wavelengths.

DODC with VetT6. The measured absorbance of 5 x $10^{-6}$ M DODC is plotted versus wavelength for a series of concentrations of VetT6 (Figure 38). Similarly to the case of DODC with 22mer, the DODC spectra with VetT6 show a decrease in $A_{max}$ with increasing DNA concentration, but there is an increase in $A_{max}$ at the highest concentration. The DODC spectra with VetT6 show a similar shift in the wavelength of $A_{max}$.

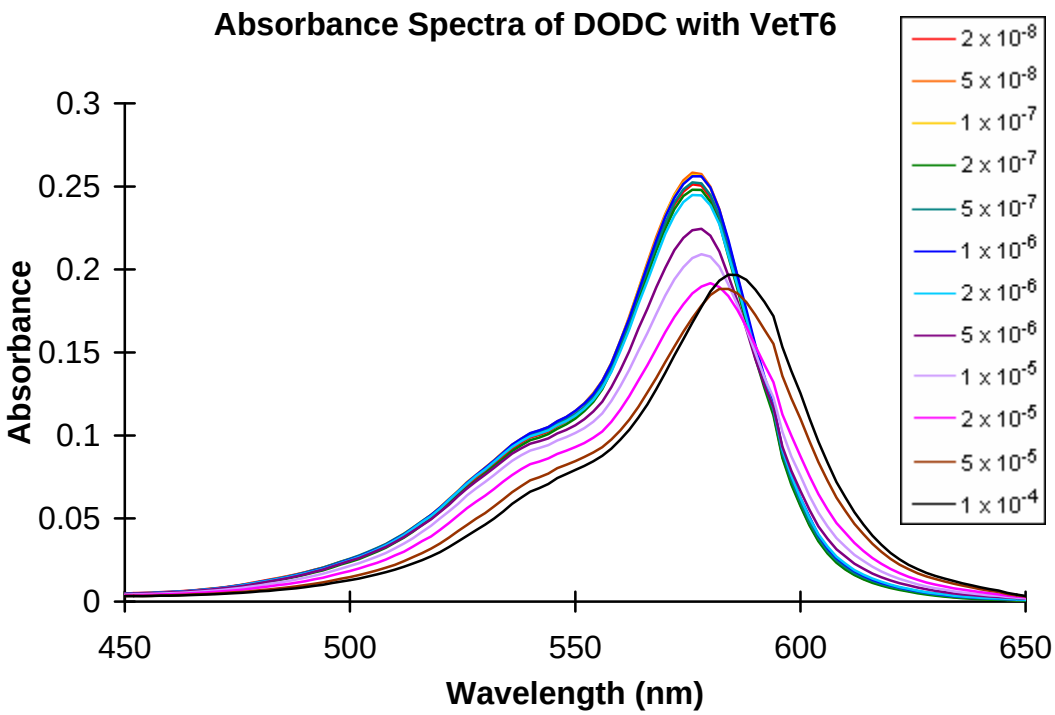


**Figure 38**. Plot of absorbance of 5 x $10^{-6}$ M DODC with VetT6 as a function of wavelength. Spectra were renormalized to 33%.

The normalized absorbance of DODC as a function of VetT6 concentration is plotted for selected wavelengths (Figure 39). The results are similar to the plots for DODC with 22mer and support the model of a single equilibrium for the binding of DODC with VetT6 between 1 x $10^{-5}$ M and 2 x $10^{-5}$ M VetT6.

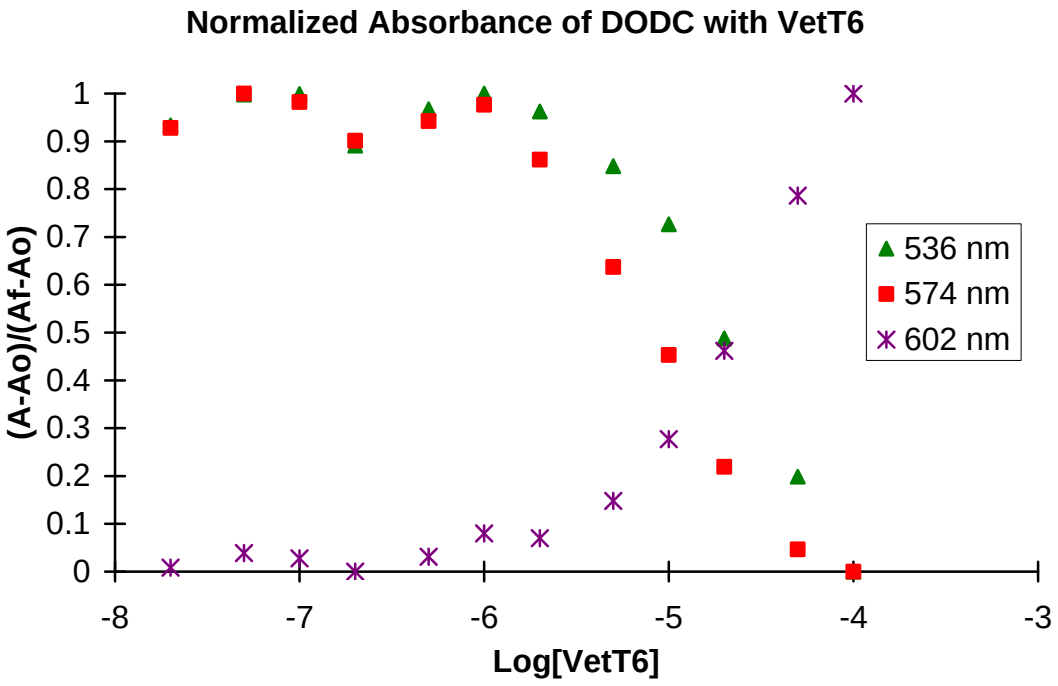


**Figure 39**. Plot of normalized absorbance, $(A-A_0)/(A_{max}-A_0)$, for 5 x $10^{-6}$ M DODC as a function of DNA concentration. The plots are of the absorbance at the indicated wavelengths.

<u>DTDC.</u> All of the DNAs induced a decrease in $A_{max}$ of DTDC up to 2 x $10^{-5}$ M DNA. High concentrations (5 x $10^{-5}$ M and 1 x $10^{-4}$ M) of 22mer and VetT4 reversed this trend and increased $A_{max}$ relative to the 2 x $10^{-5}$ M sample. Oxy1.5 induced a decrease in $A_{max}$ through the samples of highest concentration. For the

DTDC spectra with Oxy1.5, the largest drop in $A_{max}$ was between the two samples of highest concentration; this was unique to Oxy1.5. For the DTDC spectra with the remaining three DNAs, $A_{max}$ remained approximately constant for the samples of highest DNA concentration. All of the DNAs except Oxy1.5 induced a shift in $A_{max}$ towards longer wavelengths; Oxy1.5 did not induce a shift in wavelength.

DODC. All of the DNAs induced a decrease in $A_{max}$ of DODC up to 2 x $10^{-5}$ M DNA. Vet4 was the only DNA that induced a significant increase in $A_{max}$ at high concentration. Oxy1.5 and 24mer induced a continued decrease in $A_{max}$ through the samples of highest concentration. All of the DNAs induced a shift in $A_{max}$ towards longer wavelengths except Oxy1.5, which did not induce a wavelength shift.

DTDC and DODC. Both dyes showed the same variety of differences. However, the same DNA never affected both dyes in the exact same way.

| **DNA** | **Dissociation Constant ($K_d$)** | |
|---|---|---|
| | **DTDC ($10^{-5}$ M)** | **DODC ($10^{-5}$ M)** |
| 22mer | 1 | 1 - 2 |
| Vet4 | 1 | 1 - 5 |
| 24mer | 1 - 2 | 2 - 5 |
| 15mer | 1 | 1 - 2 |
| VetT4 | 0.2 - 1 | 1 - 2 |
| Oxy1.5 | 2 - 5 | 1 |
| VetU6 | | 1 - 2 |
| VetT6 | | 1 - 2 |

**Table 2.** Approximate dissociation constants of carbocyanine dyes bound to quadruplex DNAs.

As stated, carbocyanine dyes can form face-to-face dimers when in the presence of a template for aggregation. Depending on the conformation of the dimer, whether the two molecules are offset or not, the formation of a dimer can cause a

wavelength shift of the main visible absorption band in either direction. The red shift of DTDC and DODC absorption in my research is consistent with offset, or "J", aggregation. Fluorescence studies involving the same DNAs and dyes support this conclusion. Because the dG tetramers themselves are very similar among the different DNA quadruplex structures, it is possible that the dyes are binding to the loops of DNA between the dGs, which show a high degree of variation.

From this research it is clear that the two carbocyanine dyes do bind to quadruplex DNA in ways that are dependent upon both the dye and the quadruplex. The data suggest that it would be possible to use DODC and DTDC as reporter molecules, monitoring their absorption as an indicator that another molecule is binding to the quadruplex competitively.

References


1. Olovnikov, A.M., *[Principle of marginotomy in template synthesis of polynucleotides].* Dokl Akad Nauk SSSR, 1971. **201**(6): p. 1496-9.
2. Harley, C.B., A.B. Futcher, and C.W. Greider, *Telomeres shorten during ageing of human fibroblasts.* Nature, 1990. **345**(6274): p. 458-60.
3. Hanahan, D. and R.A. Weinberg, *The hallmarks of cancer.* Cell, 2000. **100**(1): p. 57-70.
4. Grandin, N. and M. Charbonneau, *Protection against chromosome degradation at the telomeres.* Biochimie, 2008. **90**(1): p. 41-59.
5. McClintock, B., *The stability of broken ends of chromosomes in Zea Mays.* Genetics, 1941. **41**: p. 234-282.
6. de Lange, T., *Shelterin: the protein complex that shapes and safeguards human telomeres.* Genes Dev, 2005. **19**(18): p. 2100-10.
7. Moyzis, R.K., et al., *A highly conserved repetitive DNA sequence, (TTAGGG)n, present at the telomeres of human chromosomes.* Proc Natl Acad Sci U S A, 1988. **85**(18): p. 6622-6.
8. Chakhparonian, M. and R.J. Wellinger, *Telomere maintenance and DNA replication: how closely are these two connected?* Trends Genet, 2003. **19**(8): p. 439-46.
9. Makarov, V.L., Y. Hirose, and J.P. Langmore, *Long G tails at both ends of human chromosomes suggest a C strand degradation mechanism for telomere shortening.* Cell, 1997. **88**(5): p. 657-66.
10. Hubscher, U., G. Maga, and S. Spadari, *Eukaryotic DNA polymerases.* Annu Rev Biochem, 2002. **71**: p. 133-63.
11. Forsburg, S.L., *Eukaryotic MCM proteins: beyond replication initiation.* Microbiol Mol Biol Rev, 2004. **68**(1): p. 109-31.
12. Porter, A.C. and C.J. Farr, *Topoisomerase II: untangling its contribution at the centromere.* Chromosome Res, 2004. **12**(6): p. 569-83.
13. Gilson, E. and V. Geli, *How telomeres are replicated.* Nat Rev Mol Cell Biol, 2007. **8**(10): p. 825-38.
14. De Cian, A., et al., *Targeting telomeres and telomerase.* Biochimie, 2008. **90**(1): p. 131-55.
15. Cesare, A.J. and R.R. Reddel, *Telomere uncapping and alternative lengthening of telomeres.* Mech Ageing Dev, 2008. **129**(1-2): p. 99-108.
16. Blasco, M.A., *Telomere length, stem cells and aging.* Nat Chem Biol, 2007. **3**(10): p. 640-9.
17. Shawi, M. and C. Autexier, *Telomerase, senescence and ageing.* Mech Ageing Dev, 2008. **129**(1-2): p. 3-10.
18. Cohen, S.B., et al., *Protein composition of catalytically active human telomerase from immortal cells.* Science, 2007. **315**(5820): p. 1850-3.
19. Gavory, G., M. Farrow, and S. Balasubramanian, *Minimum length requirement of the alignment domain of human telomerase RNA to sustain catalytic activity in vitro.* Nucleic Acids Res, 2002. **30**(20): p. 4470-80.
20. Autexier, C. and N.F. Lue, *The structure and function of telomerase reverse transcriptase.* Annu Rev Biochem, 2006. **75**: p. 493-517.

21. Bryan, T.M., et al., *Evidence for an alternative mechanism for maintaining telomere length in human tumors and tumor-derived cell lines.* Nat Med, 1997. **3**(11): p. 1271-4.
22. Bryan, T.M., et al., *Telomere elongation in immortal human cells without detectable telomerase activity.* Embo J, 1995. **14**(17): p. 4240-8.
23. Dunham, M.A., et al., *Telomere maintenance by recombination in human cells.* Nat Genet, 2000. **26**(4): p. 447-50.
24. Chang, S., et al., *Telomere-based crisis: functional differences between telomerase activation and ALT in tumor progression.* Genes Dev, 2003. **17**(1): p. 88-100.
25. Laud, P.R., et al., *Elevated telomere-telomere recombination in WRN-deficient, telomere dysfunctional cells promotes escape from senescence and engagement of the ALT pathway.* Genes Dev, 2005. **19**(21): p. 2560-70.
26. Sen, D. and W. Gilbert, *Formation of parallel four-stranded complexes by guanine-rich motifs in DNA and its implications for meiosis.* Nature, 1988. **334**(6180): p. 364-6.
27. Rujan, I.N., J.C. Meleney, and P.H. Bolton, *Vertebrate telomere repeat DNAs favor external loop propeller quadruplex structures in the presence of high concentrations of potassium.* Nucleic Acids Res, 2005. **33**(6): p. 2022-31.
28. Huppert, J.L. and S. Balasubramanian, *G-quadruplexes in promoters throughout the human genome.* Nucleic Acids Res, 2007. **35**(2): p. 406-13.
29. Sun, D., et al., *Inhibition of human telomerase by a G-quadruplex-interactive compound.* J Med Chem, 1997. **40**(14): p. 2113-6.
30. Kelland, L., *Targeting the limitless replicative potential of cancer: the telomerase/telomere pathway.* Clin Cancer Res, 2007. **13**(17): p. 4960-3.
31. Salvati, E., et al., *Telomere damage induced by the G-quadruplex ligand RHPS4 has an antitumor effect.* J Clin Invest, 2007. **117**(11): p. 3236-47.
32. Arthanari, H. and P.H. Bolton, *Functional and dysfunctional roles of quadruplex DNA in cells.* Chem Biol, 2001. **8**(3): p. 221-30.
33. Sun, H., et al., *The Bloom's syndrome helicase unwinds G4 DNA.* J Biol Chem, 1998. **273**(42): p. 27587-92.
34. Armitage, B.A.e.a., *Helical Aggregation of Cyanine Dyes on DNA Templates: Effect of Dye Structure on Formation of Homo- and Heteroaggregates.* Langmuir, 2002. **18**: p. 6330-6337.
35. Hannah, K.C. and B.A. Armitage, *DNA-templated assembly of helical cyanine dye aggregates: a supramolecular chain polymerization.* Acc Chem Res, 2004. **37**(11): p. 845-53.
36. Chen, Q., I.D. Kuntz, and R.H. Shafer, *Spectroscopic recognition of guanine dimeric hairpin quadruplexes by a carbocyanine dye.* Proc Natl Acad Sci U S A, 1996. **93**(7): p. 2635-9.
37. Luu, K.N., et al., *Structure of the human telomere in K+ solution: an intramolecular (3 + 1) G-quadruplex scaffold.* J Am Chem Soc, 2006. **128**(30): p. 9963-70.
38. De Cian, A., et al., *Reevaluation of telomerase inhibition by quadruplex ligands and their mechanisms of action.* Proc Natl Acad Sci U S A, 2007. **104**(44): p. 17347-52.

Figure 1 adapted from reference 12.
Figure 2 created by Mariana Ruiz, free use.
Figure 3 adapted from reference 13.
Figure 4 adapted from reference 14.
Figure 5 adapted from reference 27
Figure 6 adapted from references 27 and 37
Figure 7 adapted from reference 38
Figure 8 adapted from reference 35
Figure 9 adapted from reference 35